WADC TECHNICAL REPORT 52-78

STABILITY OF A WHIRLING GONDOLA SUSPENDED FROM A PARACHUTE-TESTING TOWER

GERHARD W. BRAUN
AIRCRAFT LABORATORY

JANUARY 1953

WRIGHT AIR DEVELOPMENT CENTER

NOTICES

When Government drawings, specifications, or other data are used for any purpose other than in connection with a definitely related Government procurement operation, the United States Government thereby incurs no responsibility nor any obligation whatsoever; and the fact that the Government may have formulated, furnished, or in any way supplied the said drawings, specifications, or other data, is not to be regarded by implication or otherwise as in any manner licensing the holder or any other person or corporation, or conveying any rights or permission to manufacture, use, or sell any patented invention that may in any way be related thereto.

The information furnished herewith is made available for study upon the understanding that the Government's proprietary interests in and relating thereto shall not be impaired. It is desired that the Judge Advocate (WCJ), Wright Air Development Center, Wright-Patterson Air Force Base, Ohio, be promptly notified of any apparent conflict between the Government's proprietary interests and those of others.

STABILITY OF A WHIRLING GONDOLA SUSPENDED FROM A PARACHUTE-TESTING TOWER

Gerhard W. Braun
Aircraft Laboratory

January 1953

CEO - C-03

Wright Air Development Center
Air Research and Development Command
United States Air Force
Wright-Patterson Air Force Base, Ohio

FOREWORD

The investigation described in this report was conducted by the Aerodynamics Branch of the Aircraft Laboratory, Aeronautics Division, Wright Air Development Center. The work was initiated by a Suborder dated 12 December 1951 initiated by Mr. J. H. Allen of the Equipment Laboratory, WADC. The CEO No. is C-03.

ABSTRACT

This report investigates the stability of a gondola suspended from the whirl arm of the Parachute Test Tower at El Centro, California (see Fig. 1) on which instability had been observed.

The work was started with an investigation of the pendulum oscillations of the gondola neglecting the coupling between the two modes. The result, that both frequencies become equal at approximately the speed at which the instability had been observed, was interpreted as an inclination towards instability. Therefore a more detailed investigation including the coupling between the two pendulum modes was made.

The detailed investigations showed that the damping of the pendulum modes is extremely low. Stability, however, is secured if the gondola has longitudinal static and weathercock stability and if the slope of its cross force versus angle of yaw, $\frac{\partial C_c}{\partial \beta}$, is smaller than the drag coefficient of the gondola plus cable.

Tests made on a 1:20 scale model of the parachute test tower verified the essential parts of the theoretical investigations, namely the predicted dynamic-stability, the low damping and the order of magnitude of the frequencies.

PUBLICATION REVIEW

This report has been reviewed and is approved.

FOR THE COMMANDING GENERAL:

R. G. RUEGG
Colonel, USAF
Chief, Aircraft Laboratory
Aeronautics Division

CONTENTS

LIST OF FIGURES

SYMBOLS

A_o, A_1, A_2, A_3, A_4	0	Coefficients of the frequency polynomial
a_{11}, a_{22},... a_{44}	0	Coefficients of the constant terms in the elements of the frequency polynomial
b_{11}, b_{12},...b_{44}	0	Coefficients of the linear terms in the frequency determinant
$\mathcal{C}$	(lb)	Centrifugal force
C	(lb)	Aerodynamic cross force
c_{11}, c_{12},...c_{44}	0	Coefficients of the quadratic term in the frequency determinant
$C_c = \dfrac{C}{\frac{\rho}{2} V^2 \otimes}$	0	Cross force coefficient of the gondola
C_D	0	Drag coefficient of the gondola including part of the cable drag, based on gondola cross-section.
C_m	0	Pitching moment coefficient of gondola
C_n	0	Yawing moment coefficient of gondola
D	(lb)	Drag
g	(ft/sec^2)	Acceleration caused by gravitation of the earth
$\bar{g}$	0	$= \dfrac{g}{\frac{\mathcal{L}}{2}} \mathcal{C}^2$ nondimensionalized constant of gravitation
H	(ft.lb)	Kinetic energy of the gondola
I_y, I_z	(ft.lb.sec^2)	Gondola moment of inertia about its lateral and vertical axis respectively
ℓ	(ft)	Length of gondola
$\mathcal{L}$	(ft)	Length of cable

m	lb sec^2/ft	Mass of the gondola
M	(0)	$= 1 + \dfrac{\rho_c \ell}{3m}$
N	(0)	$= \dfrac{1 + \frac{\rho_c}{2}}{1 + \frac{\rho_c}{3}}$
q_0, q_1, q_2, q_3, q_4	(rad)	Angles determining the position of the cable and the gondola in space (see Fig. 4)
Q_1, Q_2, Q_3, Q_4	ft lb	Generalized forces in the Lagrangian equation of motion
R	ft	Length of the whirling arm
t	sec	Time
$\bar{t}$	0	$= \dfrac{t}{\tau}$ nondimensionalized time
T	sec	Turning period of the whirling arm
T_1, T_2	sec	Period of the q_1 and q_2 mode respectively
v	ft/sec	Velocity of the gondola
W	lb	Weight of the gondola
x	ft	Coordinate in the direction of the cable
y	ft	Coordinate perpendicular to the direction of the cable.
α	rad.	Angle of attack of the gondola
β	rad.	Angle of yaw of the gondola
δ	ft	Deviation of the gondola path from steady state motion measured in a projection on a horizontal plane.
ζ_1, ζ_2	0	Damping factor, real part of the complex frequency, positive for stable motion
Λ	0	Length scale factor of the model
μ	0	$= \dfrac{m}{\rho \ell \otimes}$ mass factor

ν_n 0 $= -\zeta_n + \omega_n i$ complex frequency

ρ $\dfrac{lb\ sec^2}{ft^4}$ Mass density of the air

ρ_c $\dfrac{lb\ sec^2}{ft^2}$ Cable mass per length

$\bar{\rho}_c$ 0 $= \dfrac{\rho_c \mathcal{L}}{m}$ nondimensionalized cable mass

T 0 $= \dfrac{m}{\rho \otimes V}$ time factor

ω $\dfrac{rad}{sec}$ Angular velocity of the whirling arm

$\bar{\omega}$ 0 $= \omega T$ nondimensionalized angular velocity of the whirl arm

$\otimes$ ft^2 Cross section area of the gaondola

Prime ($'$) indicate derivatives with respect to $\bar{t}$

Bar ($-$) above a letter indicates either a nondimensional magnitude (see equation 32) or a vector.

Subscript zero ($_o$) indicates a magnitude belonging to the steady state condition.

INTRODUCTION

When the Service Branch of the Equipment Laboratory, WADC, operated the Parachute Test Tower at El Centro, California for the first time, a serious instability was observed at a speed of about 50 mph, that is about 1/10 of the design speed. This instability prevented further use of the equipment until the stability of the gondola could be improved.

Stability difficulties had not been expected. The test equipment had been built on the assumption that it would behave like the parachute test tower owned by Pioneer Parachute Co., Inc. which had never shown any difficulties resulting from instability. The two parachute test towers, that at El Centro and that of Pioneer Parachute Co., however, are remarkably different in size and are not dynamically similar to each other.

The motion performed by the gondola after a disturbance had not yet been studied either by systematic tests or by analytical investigations. It was obvious, however, that the motion of the gondola had a certain similarity to the motion of airplanes. Therefore the Aircraft Laboratory, WADC, was requested to perform a stability investigation.

THE EQUIPMENT

The gondola which will be investigated stabilitywise houses a parachute and a dummy of a man. The gondola is designed to be whirled around a vertical axis with speeds up to 500 mph. The parachute and the dummy are released when the desired speed is reached.

The dimensions of this parachute testing equipment are given in Fig. 1 and 2. The whirling arm has a length of 56 feet and extends horizontally 120 ft above the ground. The arm is driven by an electric motor of 2800 HP controlled by the Ward Leonard system. Between the shaft of the driving motor and the axis of the whirling arm there is a gear reduction of 22:1. This high gear reduction makes the whirl arm self locking. A disturbance of the gondola will not affect the angular velocity of the arm.

The gondola has a diameter of 28" and is 112" long (see Fig. 2). The center of gravity of the gondola is located 41% of its length behind its nose. Static longitudinal stability and weathercock stability is secured by tailplanes. The gondola is open on its bottom which increases the drag of the gondola considerably. The weight of the loaded gondola is W_λ = 685 lbs, its empty weight is W_e = 405 lbs.
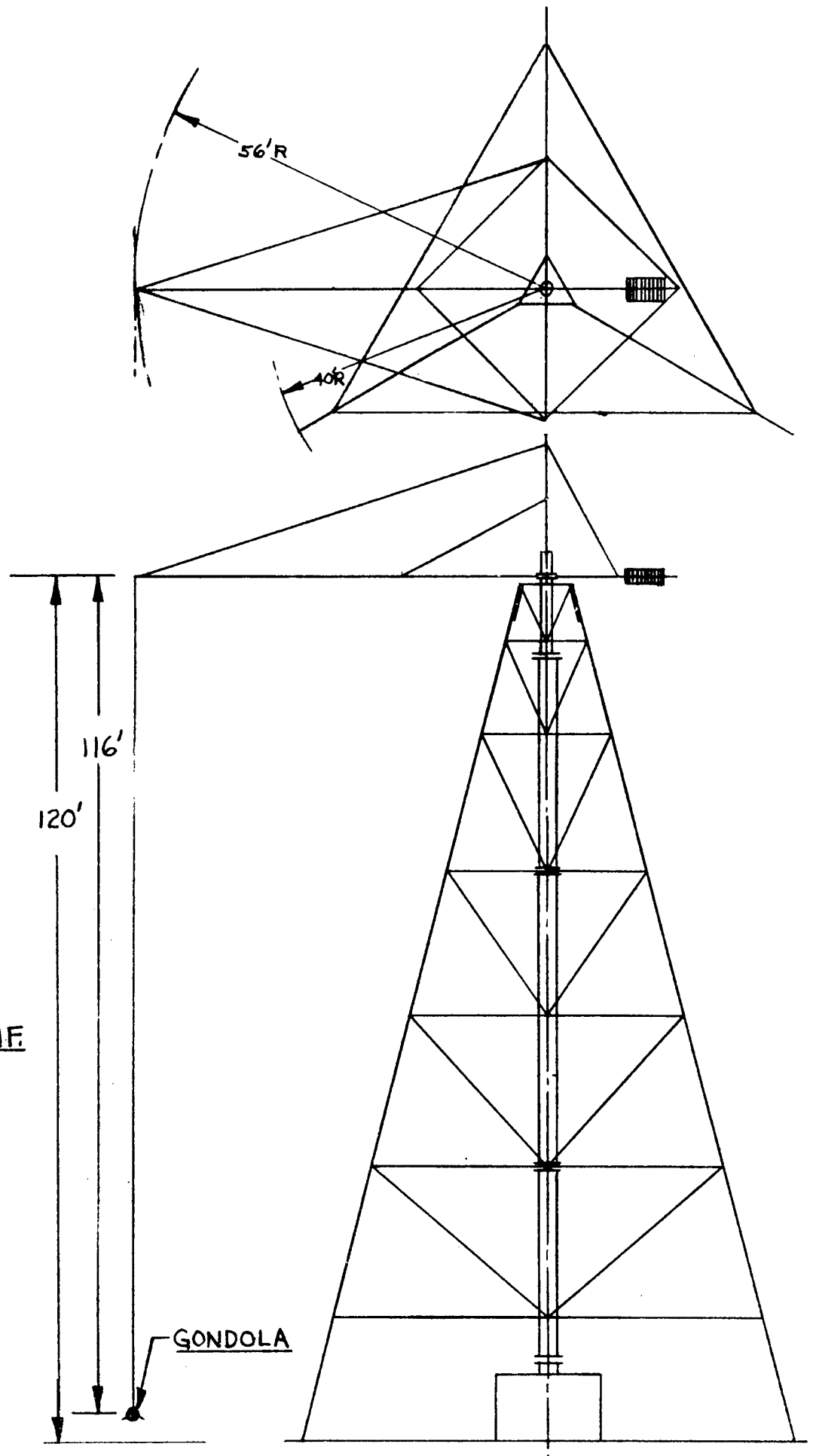
FIG. 1.
PARACHUTE
TEST TOWER
EL CENTRO, CALIF.

56'R

40'R

116'

120'

GONDOLA

FIG. 3 CABLES & SHEATHING CROSS SECTION WITH WHICH
INSTABILITY HAD BEEN OBSERVED.
SCALE: TWICE SIZE.

NACA 0020-G4 AIRFOIL
CHORD LENGTH = 4.25"

.449 DIA. TYP.

14"R.

29"R.
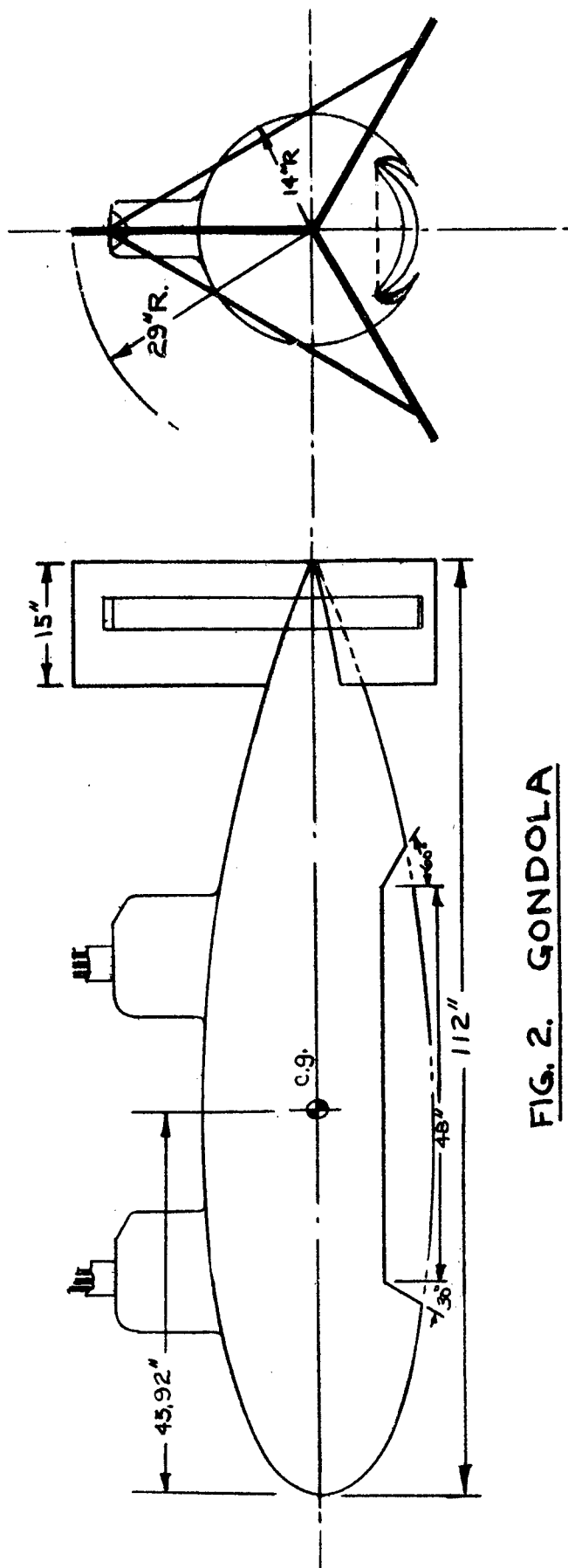
FIG. 2. GONDOLA
SCALE: 1/20 SIZE

15"

c.g.

45.92"

112"

48"

30"

The gondola is suspended from the end of the whirl arm by one or more cables of 116 feet length. During the runs showing the instability, a six cable suspension was used. These 6 cables were housed in two stream-lined sheathings, each including 3 cables. The profile of the sheathings was NACA 0020-63. Fig. 3 shows a cross section through the sheathing and the cables. The two cable units were attached 19 inches in front of and to the rear of the center of gravity of the gondola.

THE PROBLEM

A solid body moving freely in space has 6 degrees of freedom. In the present case of the gondola, one degree of freedom is eliminated by the cable, if one assumes that the cable is always kept taut. This assumption is made throughout the following investigations.

The remaining five degrees of freedom are coupled with each other in a manner remarkably different from the free flight conditions. Therefore the experience gained on free flying aircrafts and models cannot be applied to the stability problem of the gondola. The equations of motion must be adapted to the present case and solved anew.

It is the purpose of the investigation at hand to analyze the motion, to find out which conditions might cause instability and which precautions prevent instability, and finally to check the theoretical results qualitatively by model tests.

The five rigid body degrees of freedom of the gondola may be described by five angles shown in Fig. 4.

$q_{10} + q_1$ = the angle of the cable measured in a radial plane, that is a vertical plane including the arm; q_{10} is the component which belongs to the steady state conditions. It can be calculated as a function either of the circumferential velocity or of the angular velocity, ω, of the whirl arm.

q_2 = the angle between the cable and the radial plane, measured in a tangential plane. Precisely speaking there is also a steady state component q_{20} due to the drag of the cable and the gondola, but q_{20} is small and will be neglected in this calculation.

q_3 = the angle of pitch of the gondola measured in the tangential plane from the horizon. If the gondola is trimmed accurately the steady state value q_{30} is zero.

Fig. 4a - The "Tangential Plane" and the "Radial Plane"

The "Radial Plane" is a vertical plane including the arm OP.

The "Tangential Plane" is a plane containing the end point P of the arm and the tangent of the undisturbed flight path.

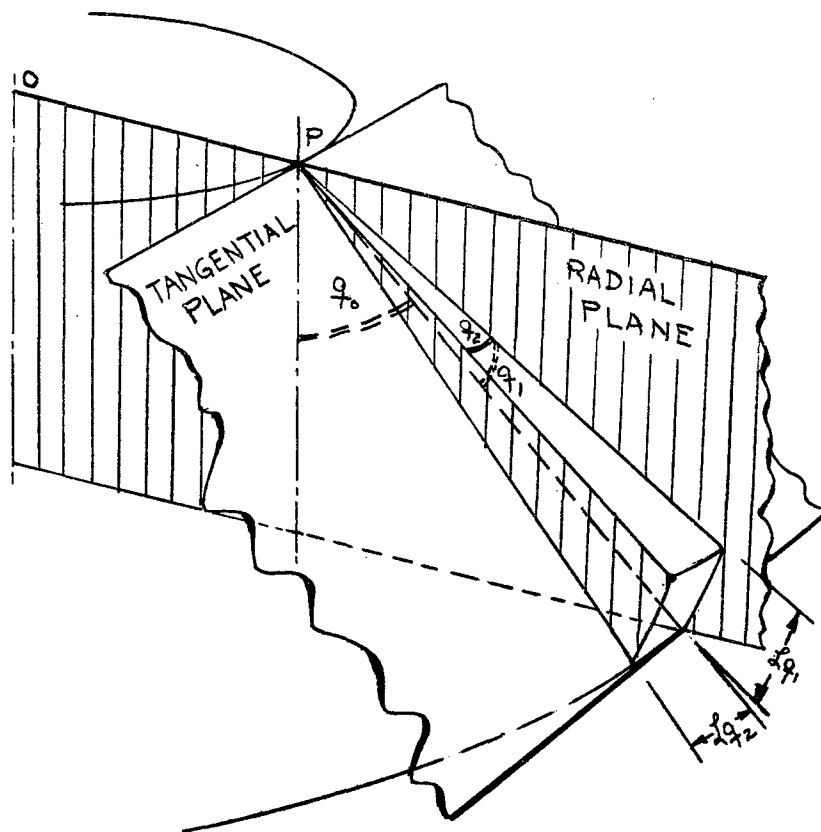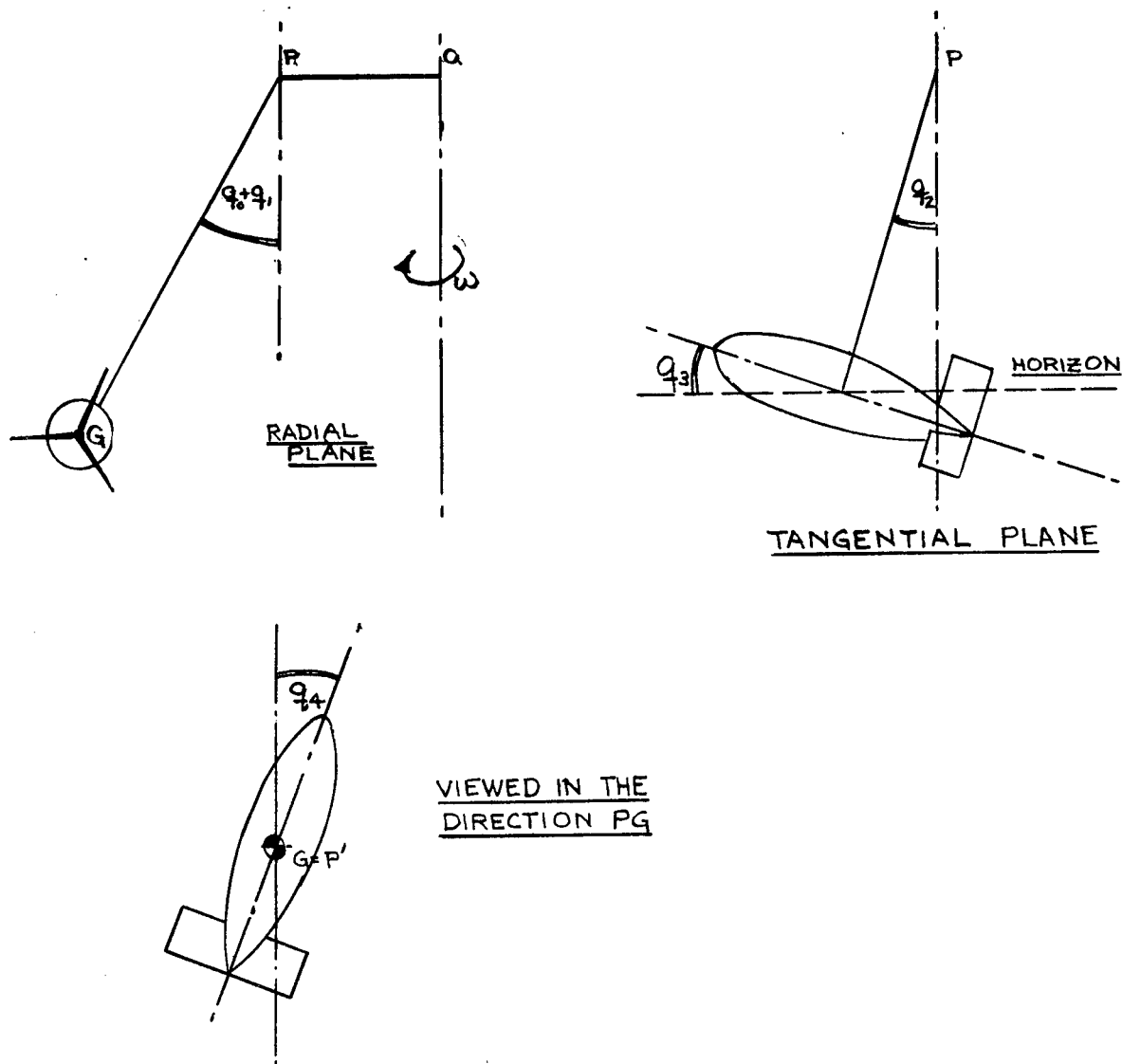Fig. 4b – Definition of the angles q_p, q_1, q_2, q_3, q_4, describing the position in space of the gondola.

q_4 = the angle between the gondola axis and the tangent on the undisturbed flight path measured in a horizontal plane. If the point of attachment is different from the center of gravity of the gondola the centrifugal force will produce a permanent angle of yaw q_{40}. The same may be caused by unsymmetry of the model or by rudder deflection. In the calculations q_{40} is assumed to be zero.

q_5 = the angle of roll measured from the position where the c.g. of the gondola is in line with the direction of the cable-end-tangent.

Precisely speaking, these are not all the degrees of freedom since the cable has the possibility of moving with an infinite number of mode shapes. These motions can be split up into two components located in the directions of q_1 and q_2.

The basic mode shape is very similar to a straight line represented by the cable with an amplitude q_1 and q_2. The higher mode shapes have nodes and will not be included in the present analysis. They may be added later in a more extended investigation, if this is required.

A decision had to be made about the type of cable suspension to be investigated. The tandem arrangement of the cable units was suspected from the beginning as a possible cause of the observed instability. Therefore a mathematical verification of the instability might be of interest. The following reasons, however, prevented the investigation of the double suspension. The cable sheathing was so designed that the aerodynamic center of pressure was located behind the center of gravity of the sheathing and the included cables. Consequently the cable sheathing would be twisted and high crosswise aerodynamic forces would be produced on the sheathing which could not be neglected. A sufficiently accurate treatment of these forces, however, would not be possible, since the irregular initial distribution of the twist angle along the cables was not known and no data were available about the friction between the different assembly units of sheathing. In addition, the mutual aerodynamic interaction between the sheathing of the two cable units would have complicated the calculations. The results, moreover, would have been of academic interest only, since it had already been decided to use in the future a single cable suspension. Therefore, this investigation is confined to the single cable suspension.

THEORETICAL INVESTIGATIONS

Performance Considerations

The stability investigation will show that the damping of a gondola disturbance is proportional to the drag coefficient of the gondola and cable. Consequently the highest drag would provide the best stability. Therefore it is of interest to find the highest drag coefficient compatible with the required speed of 500 mph.

For lower speeds the cable angle depends upon the speed. Consequently in the low speed range an exact performance calculation becomes involved. Fortunately, only high speed cases are of interest for performance considerations. For these cases, however, the cable can be assumed stretched horizontally. This assumption has been made in the following calculations.

The total drag of the rotating system is composed of the drag of the gondola, the suspension cable, the pipes and wires composing the whirl arm, and its supports.

All drag components are assumed in the form

$$D_n = \frac{\rho}{2} C_D \int_{x_1}^{x_2} x^2 \omega^2 d\, (dx)$$

where ρ is the mass density of air, C_D the local drag coefficient, which is assumed independent from Reynolds and Mach number, x is the distance of a point from the center of rotation, d is the diameter of the part, ω is the angular velocity of the whirl arm. The dimensions of the framework have been substituted as given in the stress analysis of the tower. The gondola suspension has been assumed as a single cable of 1-7/8 inch diameter. The drag coefficient of all cables and steel tubes has been assumed to be 1.25 based on their frontal area. The drag coefficient of the gondola is assumed to be 0.2 based on its main cross section.

The result of these calculations are plotted in Fig. 5. The upper curve refers to the unsheathed cable, the lower curve to a sheathed cable with the drag coefficient $C_D = .24$ based on the cable cross section.

The drag of the unsheathed cable causes 87% and the gondola 6-1/2% of the total required power.
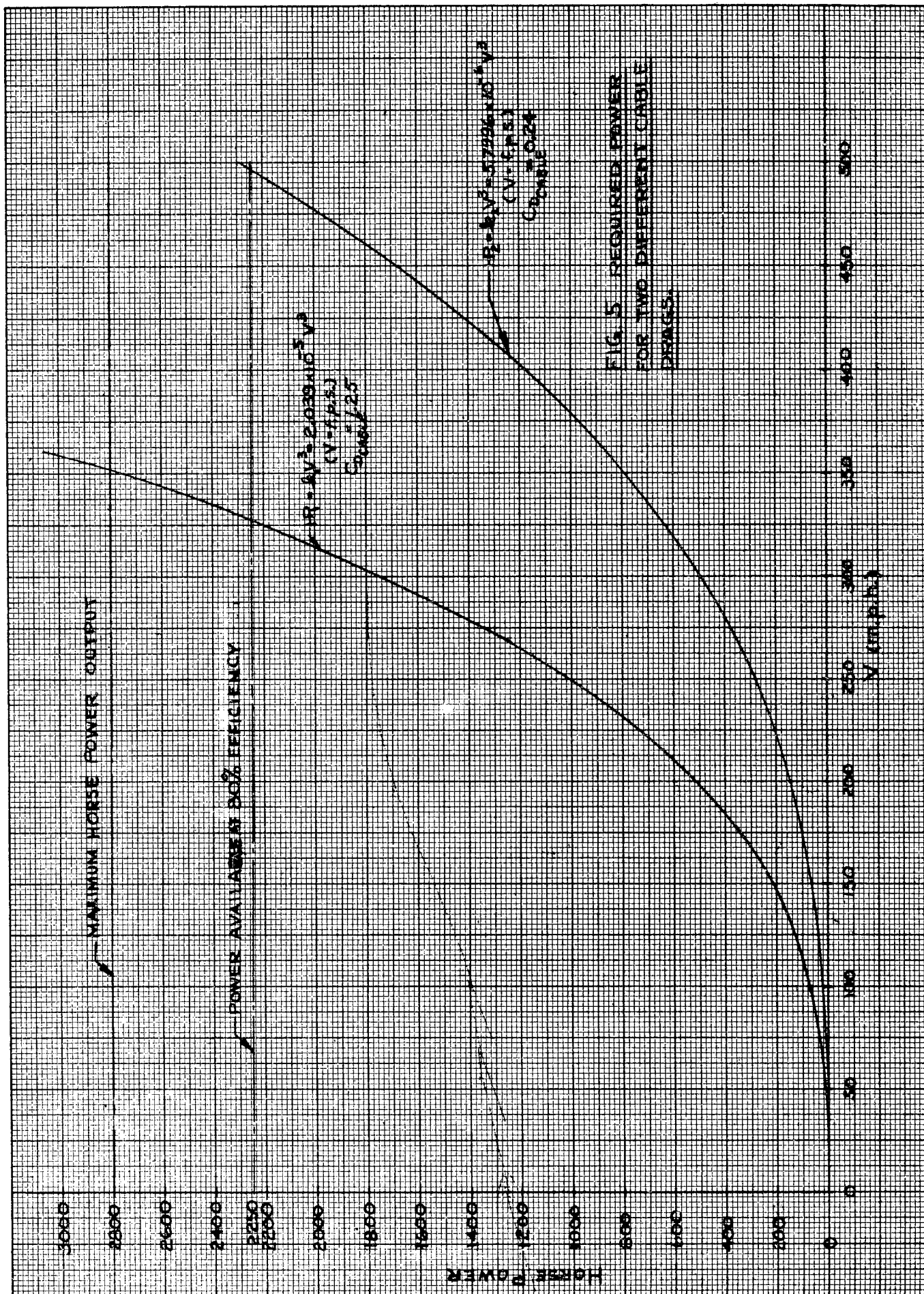
FIG. 5 REQUIRED POWER
FOR TWO DIFFERENT CABLE
DRAGS.

$R = 4_2 v^3 = 2.039 \times 10^{-5} \; V^3$
$(V = f.p.s.)$
$C_{DCABLE} = 1.25$

$R_2 = 4_2 v^3 = 5.722 \times 10^{-4} \; V^3$
$(V = f.p.s.)$
$C_{DCABLE} = .024$

MAXIMUM HORSE POWER OUTPUT

POWER AVAILABLE AT 80% EFFICIENCY

The lower drag coefficient of C_D = .24 can be realized by using a triangular sheathing as shown in Fig. 6. This type of sheathing is considered cheap in manufacturing cost and upkeep.
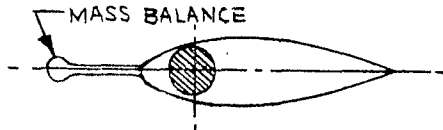
Triangular Sheathing

A still lower drag coefficient can be obtained by using a regular symmetrical wing profile. This, however, will require a mass balance and is considered more expensive than the triangular sheathing.

Wing Profile Sheathing

Fig. 6 Forms of dynamically stable Sheathings

The available power is also shown in Fig. 5. The output of the driving motor is 2800 HP and the maximum power on the whirling arm is 2240 HP, if a loss of 20% in the total driving mechanism is assumed.

The graph indicates that the required gondola speed of 500 mph can be obtained, if the drag coefficient of the cable is not higher than .24.

Shape of the Cable Under Steady Motion

The knowledge of the shape of the cable under steady state conditions is important. Only if this shape is known can reasonable approximations be found and justified. To begin with, the shape of the cable in the radial plane will be calculated. This is determined by the weight and the centrifugal forces.

In order to obtain simple conditions, this problem is solved in two steps. First the equilibrium position of the cable is calculated under the assumption that it is a straight line. Secondly the deviation from the straight line is calculated and it is shown that this deviation is small.

a. <u>Equilibrium position under the assumption of a straight line</u> <u>cable shape.</u>
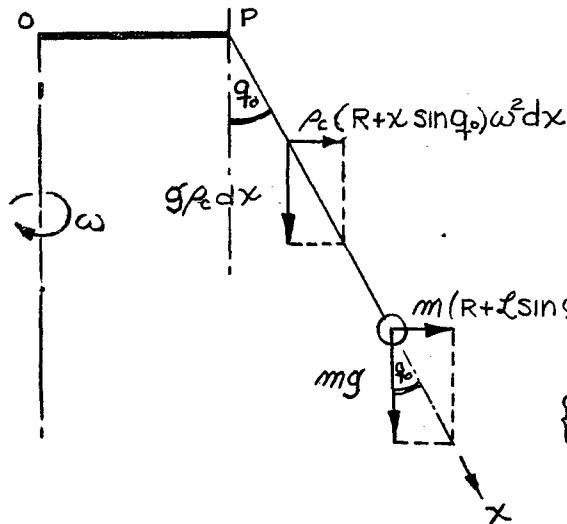
The coordinate along the cable is called x . The origin of the coordinates is put at the end point P of the whirl arm.

Equilibrium is obtained, if the sum of the moments about point P vanishes. This condition gives the equation

$$\left\{ m\left(R+\mathcal{L}\sin q_0\right)\mathcal{L}\cos q_0 + \int_0^{\mathcal{L}}\rho_c\left(R+x\sin q_0\right)x\cos q_0\,dx\right\}\omega^2 = mg\mathcal{L}\sin q_0 + \int_0^{\mathcal{L}}\rho_c g x\sin q_0\,dx$$

Fig. 7 Cable forces for the assumption of a straight cable shape

$$\left\{\frac{m}{\rho_c}\left(R+\mathcal{L}\sin q_0\right)+\frac{R\mathcal{L}}{2}+\frac{\mathcal{L}^2}{3}\sin q_0\right\}\omega^2 = g\left(\frac{m}{\rho_c}+\frac{\mathcal{L}}{2}\right)\tan q_0 \tag{1}$$

or

$$\omega^2 = \frac{g\left(\frac{m}{\rho_c}+\frac{\mathcal{L}}{2}\right)\tan q_0}{\frac{m}{\rho_c}\left(R+\mathcal{L}\sin q_0\right)+\frac{R\mathcal{L}}{2}+\frac{\mathcal{L}^2}{3}\sin q_0} \tag{2}$$

The numerical relation between ω and q_0 as obtained by evaluation of equation (2) has been plotted in Fig. 8. One sees as long as the angular velocity is small the angle q_0 changes rapidly with ω. At higher ω however, q_0 changes very little and approaches 90° asymptotically.
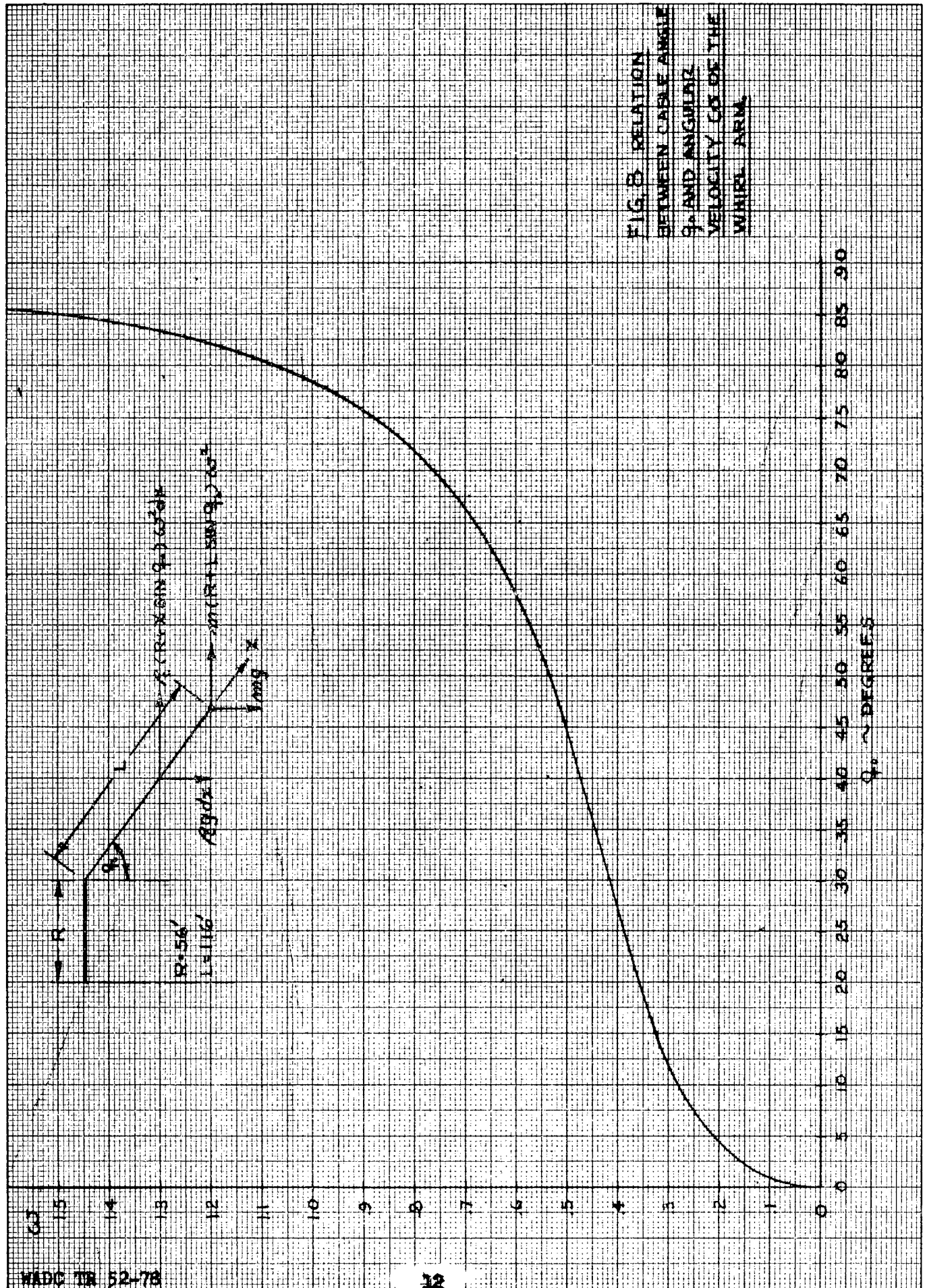
FIG. 8 RELATION BETWEEN CABLE ANGLE φ_o AND ANGULAR VELOCITY ω OF THE WHIRL ARM.

b. __Deviation of cable shape from straight line.__

Fig. 9   Coordinate system for
curved cable shape
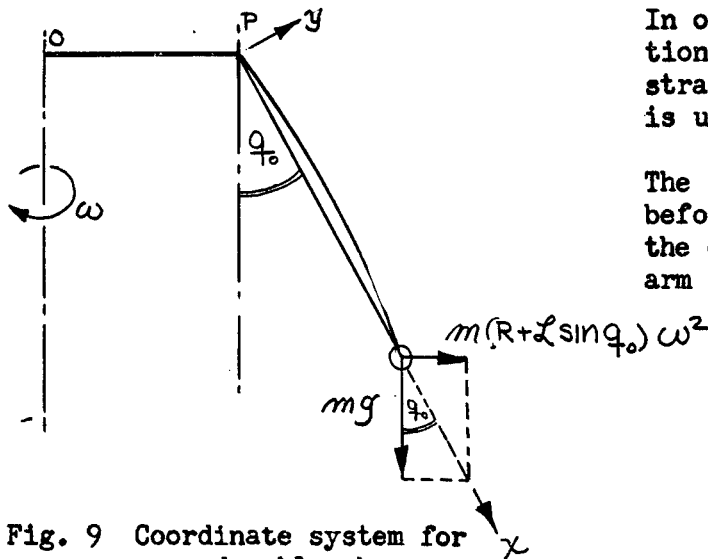
In order to designate the devia-
tion of the cable shape from the
straight line, the coordinate y
is used.

The coordinate x is the same as
before (Fig. 7). It extends from
the end point, P, of the whirling
arm to the center of the gondola.

Since the x axis has already the average direction of the cable,
the cable slope $\frac{dy}{dx}$ will be small. Consequently the length element
is

$$ds = \sqrt{dx^2 + dy^2} \approx dx$$

The components of the cable tension in x and y directions are

$$T_x = \left\{ m(R + \mathcal{L}\sin q_o) + \rho_c \left(R\mathcal{L} + \frac{\mathcal{L}^2}{2}\sin q_o - Rx - \frac{x^2}{2}\sin q_o \right) \right\} \omega^2 \sin q_o$$
$$+ \left\{ m + (\mathcal{L}-x)\rho_c \right\} g \cos q_o \tag{3}$$

$$T_y = \left\{ m(R + \mathcal{L}\sin q_o) + \rho_c \left(R\mathcal{L} + \frac{\mathcal{L}^2}{2}\sin q_o - Rx - \frac{x^2}{2}\sin q_o \right) \right\} \omega^2 \cos q_o$$
$$- \left\{ m + \rho_c(\mathcal{L}-x) \right\} g \sin q_o \tag{4}$$

Remembering that $\left\{ m(R + \mathcal{L}\sin q_o) + \rho_c \left(\frac{R\mathcal{L}}{2} + \frac{\mathcal{L}^2}{3}\sin q_o \right) \right\} \omega^2 \cos q_o$

$$- (m + \rho_c \frac{\mathcal{L}}{2}) g \sin q_o = 0$$

equation (4) can also be written

$$T_y = \rho_c \left[\begin{array}{c} (\frac{R\mathcal{L}}{2} + \frac{\mathcal{L}^2}{6}\sin q_0)\,\omega^2\cos q_0 - \frac{\mathcal{L}}{2}g\sin q_0 \\[2mm] -(Rx + \frac{x^2}{2}\sin q_0)\,\omega^2\cos q_0 + xg\sin q_0 \end{array} \right]$$

In this form it is easily seen that T_y changes its sign in the neighborhood of $x = \frac{\mathcal{L}}{2}$, which indicates that the cable curve can not deviate too much from the straight line.

The differential equation of the cable curve is

$$\frac{dy}{dx} = \frac{T_y}{T_x} \tag{5}$$

which gives after factoring $\dfrac{\cos q_0}{\sin q_0}$

$$y = \cot q_0 \int_0^x \frac{\{m(R+\mathcal{L}\sin q_0)+\rho_c(R\mathcal{L}+\frac{\mathcal{L}^2}{2}\sin q_0)\}\omega^2-(m+\rho_c\mathcal{L})g\tan q_0 - \rho_c(R\omega^2-g\tan q_0)x - \frac{\rho_c}{2}\omega^2\sin q_0\,x^2}{\{m(R+\mathcal{L}\sin q_0)+\rho_c(R\mathcal{L}+\frac{\mathcal{L}^2}{2}\sin q_0)\}\omega^2+(m+\rho_c\mathcal{L})g\cot q_0 - \rho_c(R\omega^2+g\cot q_0)x - \frac{\rho_c}{2}\omega^2\sin q_0\,x^2} dx$$

The x^2 term in the denominator is removed by dividing by the numerator:

$$y = \cot q_0 \int_0^x \left[1 + \frac{g(\tan q_0+\cot q_0)\left[-(m+\rho_c\mathcal{L})+\rho_c x\right]}{\{m(R+\mathcal{L}\sin q_0)+\rho_c(R\mathcal{L}+\frac{\mathcal{L}^2}{2}\sin q_0)\}\omega^2 + (m+\rho_c\mathcal{L})g\cot q_0 - \rho_c[R\omega^2+g\cot q_0)x - \frac{\rho_c}{2}\omega^2\sin q_0 x^2} \right] dx$$

After splitting the fraction up into linear partial fractions and integrating, one obtains

$$y = \cot q_0 \left\{ x - \frac{g(\tan q_0+\cot q_0)}{\rho_c}\left[K_1\ln(1-\frac{x}{\alpha}) + K_2\ln(1-\frac{x}{\beta}) \right] \right\} \tag{6}$$

$$K_1 = \frac{a + \alpha b}{\alpha - \beta}$$

$$K_2 = - \frac{a + \beta b}{\alpha - \beta}$$

$$a = - (m + \rho \mathcal{L})$$

$$A = \left\{ m(R + \mathcal{L} \sin q_0) + \rho \left(R\mathcal{L} + \frac{\mathcal{L}^2}{2} \sin q_0 \right) \right\} \omega^2 + (m + \rho \mathcal{L}) g \cot q_0$$

$$b = \rho_c$$

$$B = \rho_c \left[R \omega^2 + g \cot q_0 \right]$$

$$\mathcal{C} = \frac{\rho_c}{2} \omega^2 \sin q_0$$

$$\alpha = - \frac{B}{2\mathcal{C}} + \sqrt{\left(\frac{B}{2\mathcal{C}} \right)^2 - \frac{A}{\mathcal{C}}}$$

$$\beta = - \frac{B}{2\mathcal{C}} - \sqrt{\left(\frac{B}{2\mathcal{C}} \right)^2 - \frac{A}{\mathcal{C}}}$$

The shape of the cable is plotted in Fig. 10 for $q_0 = 45°$, the angle at which the maximum curvature of the cable can be expected. One sees that the deviation from the straight line is less than 1% of its length. The substitution of the cable shape by a straight line is thus justified.
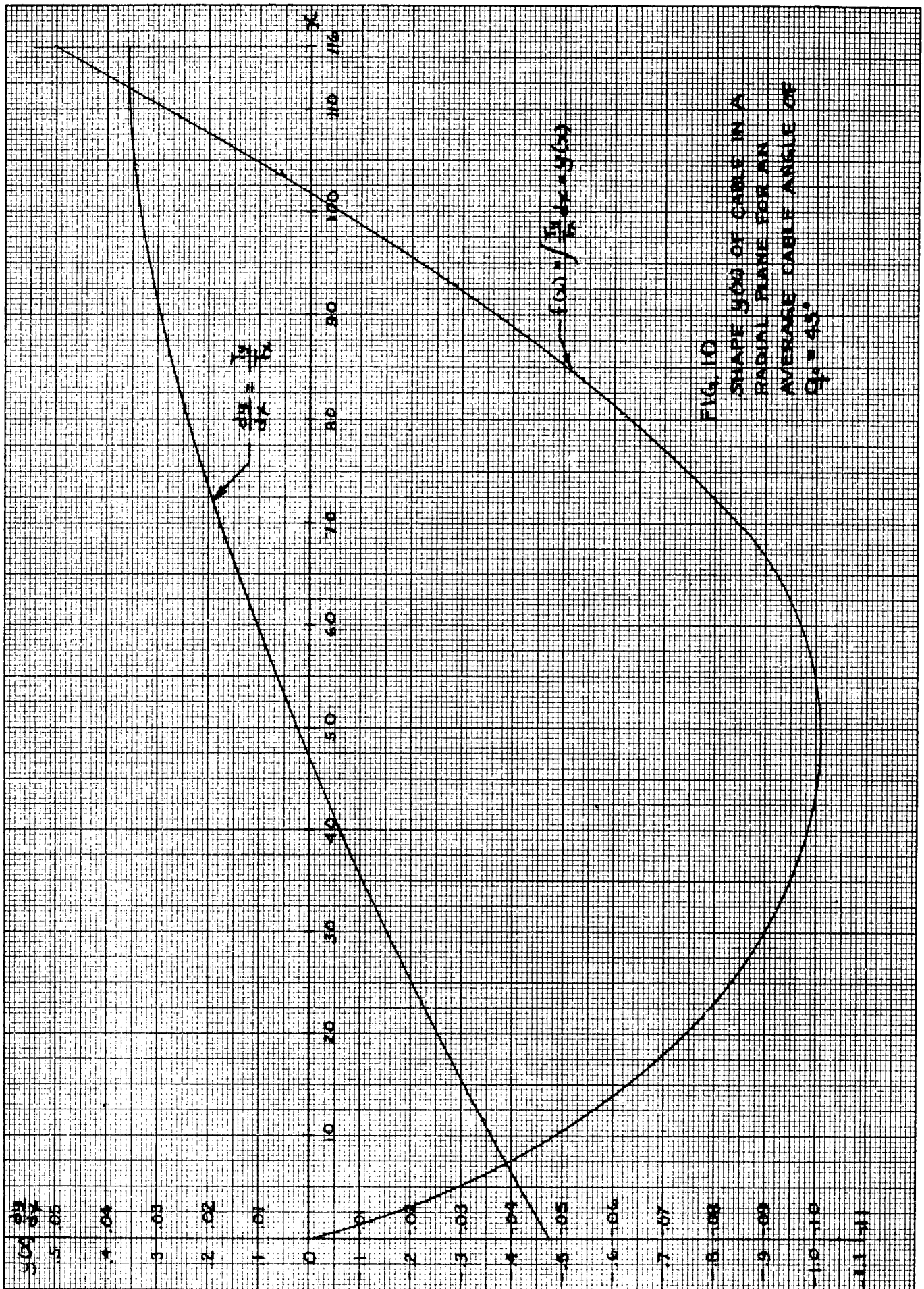
FIG. 10

SHAPE $y(x)$ OF CABLE IN A
RADIAL PLANE FOR AN
AVERAGE CABLE ANGLE OF
$\bar{q}_a = 45°$

$$f(x) = \sqrt{\frac{h}{K}} e^x = y(x)$$

$$\frac{dy}{dx} = \frac{dy}{dx}$$

The Pendulum Modes Treated As Uncoupled Degrees of Freedom

   a. **Outward-Inward Oscillations**: This motion is restricted to the radial plane (Fig. 4a). The forces acting are the weight, the centrifugal forces and the cross forces on the gondola. Assuming that the gondola has a high enough weathercock stability, the gondola will turn its nose always into the resultant wind so that the cross forces become zero. Therefore the airforces will be neglected in the treatment of the uncoupled motion.

The total moment about the point of suspension, P, is

$$M = \left\{ m\left[R + \mathcal{L}\sin(q_0 + q_1)\right]\mathcal{L} + \mathcal{A}\left[R\frac{\mathcal{L}^2}{2} + \frac{\mathcal{L}^3}{3}\sin(q_0 + q_1)\right]\right\} \omega^2 \cos(q_0 + q_1)$$
$$- \left\{ m\mathcal{L} + \mathcal{A}_c \frac{\mathcal{L}^2}{2}\right\} g\sin(q_0 + q_1)$$

The equation of motion

$$\left(m\mathcal{L}^2 + \mathcal{A}_c \frac{\mathcal{L}^3}{3}\right)\ddot{q}_1 - \frac{\partial M}{\partial q_1} q_1 = 0$$

becomes

$$\left(m\mathcal{L}^2 + \frac{\mathcal{A}\mathcal{L}^3}{3}\right)\ddot{q}_1 + \left[\left(m\mathcal{L} + \mathcal{A}\frac{\mathcal{L}^2}{2}\right)g\cos q_0 + \left\{m(R + \mathcal{L}\sin q_0)\mathcal{L}\right.\right.$$
$$\left.+ \mathcal{A}\left(R\frac{\mathcal{L}^2}{2} + \frac{\mathcal{L}^3}{3}\sin q_0\right)\right\}\omega^2 \sin q_0 - \left\{m\mathcal{L}^2 + \mathcal{A}\frac{\mathcal{L}^3}{3}\right\}\cos^2 q_0\,\omega^2\right]q_1 = 0$$

or
$$\ddot{q}_1 + \left\{\frac{m + \mathcal{A}\frac{\mathcal{L}}{2}}{m + \mathcal{A}\frac{\mathcal{L}}{3}}\frac{g}{\mathcal{L}}\cos q_0 - \cos^2 q_0\,\omega^2 + \frac{m(\frac{R}{\mathcal{L}} + \sin q_0) + \mathcal{A}\mathcal{L}(\frac{R}{2\mathcal{L}} + \frac{1}{3}\sin q_0)}{m + \mathcal{A}\frac{\mathcal{L}}{3}}\,\omega^2 \sin q_0\right\}q_1 = 0$$

The related frequency is

$$\nu_1 = \omega\sqrt{\left[\frac{m + (\frac{R}{\mathcal{L}} + \sin q_0) + \mathcal{A}\mathcal{L}(\frac{R}{2\mathcal{L}} + \frac{1}{3}\sin q_0)}{m + \mathcal{A}\frac{\mathcal{L}}{3}}\sin q_0 - \cos^2 q_0\right] + \frac{m + \mathcal{A}\frac{\mathcal{L}}{2}}{m + \mathcal{A}\frac{\mathcal{L}}{3}}\frac{g}{\mathcal{L}}\frac{\cos q_0}{\omega^2}} \quad (8)$$

The period $T_{1u} = \frac{2\pi}{\nu_1}$ is plotted versus the whirling frequency in Fig. 11, where it is marked T_{1u}.

   The period of the uncoupled outward-inward pendulum motion reaches about 90% of the whirling period.

   b. **Fore and aft oscillations**: This type of oscillation occurs in the tangential plane. The restoring forces are again given by the components of forces related to the gravitational and the centrifugal forces.

FIG. 11. WHIRLING PERIOD T AND PENDULUM
PERIODS T₁ AND T₂ AS FUNCTIONS OF THE
CABLE ANGLE θₒ.
T₁ᵤ, T₂ᵤ   PERIODS FOR UNCOUPLED MOTION
T₁ₒ, T₂ₒ   PERIODS FOR COUPLED MOTION
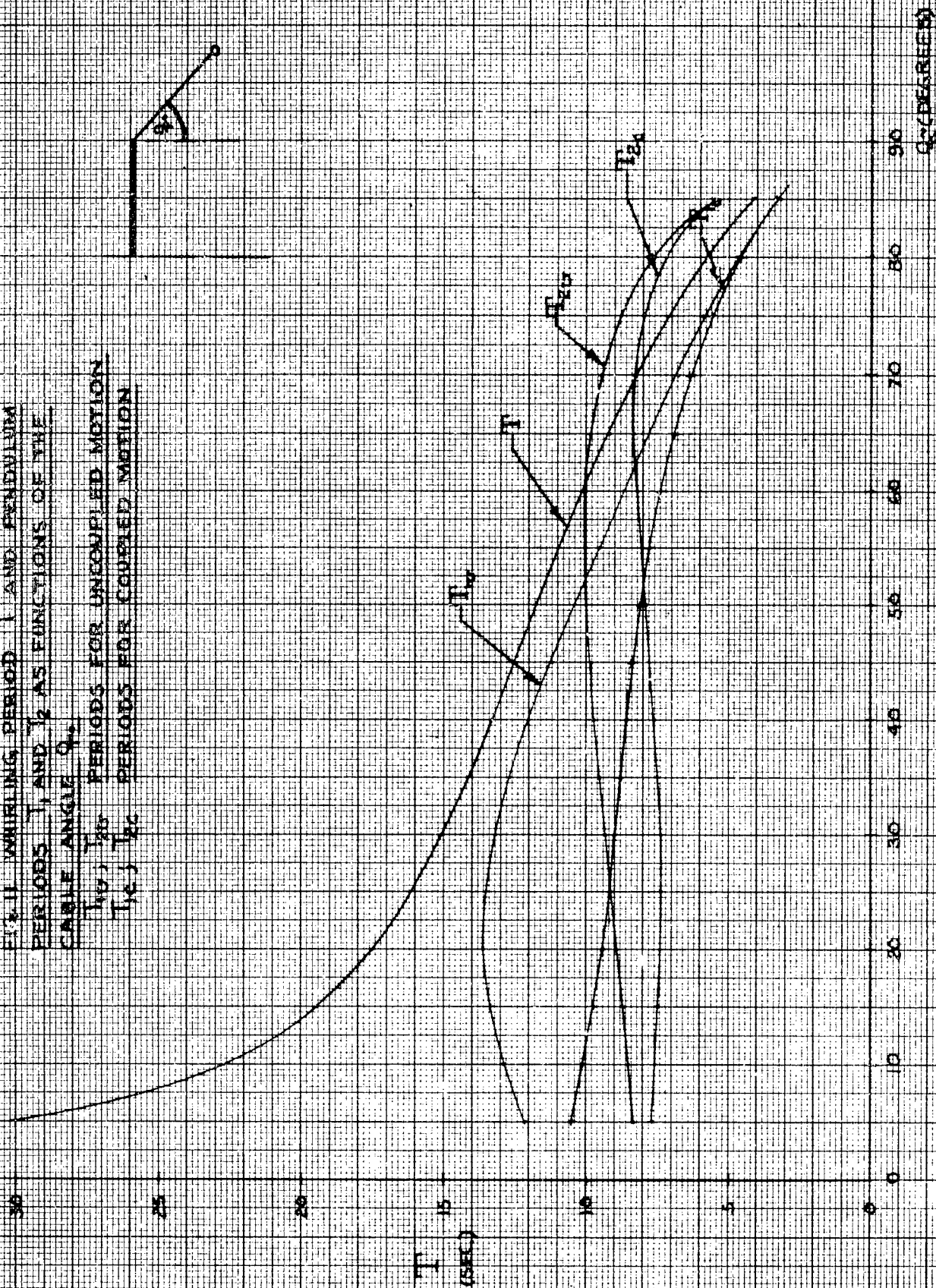
Coriolis forces do not enter the investigation of the uncoupled oscillations, since these are typical coupling forces.

The restoring moment is produced by the gravitational forces and by the centrifugal forces. The centrifugal forces act horizontally and point in a direction away from the axis of rotation. The centrifugal forces can be resolved into two components, one producing a moment tending to restore q_2, to zero, the other producing a cable force and a moment which tries to increase q_1. (See Fig. 13)

The restoring moment produced by the centrifugal force on the gondola is $m[R + \mathcal{L}\sin(q_0 + q_1)]\omega^2 \sin\beta' \cdot \mathcal{L}$ where β' is the angle defined later in Fig. 14 and in equation 15. Substituting the value for $\sin\beta'$ and adding the contribution of the cable one obtains the total restoring moment:

$$M_2 = -\left[\frac{mR\mathcal{L}\omega^2}{\sin q_0} + \int_0^{\mathcal{L}}\frac{\mathcal{R}xR\omega^2}{\sin q_0}dx + mg\cos q_0\,\mathcal{L} + \int_0^{\mathcal{L}}\mathcal{R}xg\cos q_0\,dx\right]q_2$$

$$= -\left(m + \frac{\mathcal{R}\mathcal{L}}{2}\right)\left(\frac{R\mathcal{L}\omega^2}{\sin q_0} + g\cos q_0\,\mathcal{L}\right)$$

The equation of motion is

$$\left(m\mathcal{L}^2 + \frac{\mathcal{R}\mathcal{L}^3}{3}\right)\ddot{q}_2 + \left(m + \frac{\mathcal{R}\mathcal{L}}{2}\right)\left(\frac{R\omega^2}{\sin q_0} + g\cos q_0\right)\mathcal{L}\,q_2 = 0$$

which has the frequency

$$\nu = \sqrt{\frac{m + \mathcal{R}\frac{\mathcal{L}}{2}}{m + \mathcal{R}\frac{\mathcal{L}}{3}}\left(\frac{R}{\mathcal{L}\sin q_0} + \frac{g\cos q_0}{\mathcal{L}\omega^2}\right)}\;\omega \qquad (9)$$

The period $T_{2u} = \dfrac{2\pi}{\nu_2}$ is also plotted in Fig. 11. For $q_0 = 5°$, T_{2u} starts out with less than 1/3 of the value of T and becomes higher than T for q_0 greater than 60°.

The fact that all three periods T_1, T_2, and T are of the same order of magnitude leads one to expect strong couplings. This will make the evaluation of tests difficult unless one of the two modes is much more damped than the other. It also makes an investigation of the coupled motion necessary.

Derivation of the Equations of Coupled Motion

The investigation of the stability of the steady state motions of the gondola is the main purpose of the present report. This will be done on the basis of the theory of vibrations developed by Lagrange.

The degrees of freedom considered are described by the coordinates q_1, q_2, q_3, q_4, which have been introduced before. This means that the rolling motions of the gondola and the torsional and translational motion of the cable in itself, which do not affect the position of the cable ends, are neglected.

In order to eliminate the internal forces produced by the cable, the equations of motion will be used in the Lagrangian form. Using the symbol H for the kinetic energy and Q_1, Q_2, Q_3, Q_4 for the generalized forces belonging to the degrees of freedom q_1, q_2, q_3, q_4, respectively, the Lagrangian equation of motion can be written:

$$\frac{d}{dt}\frac{\partial H}{\partial \dot{q}_1} - \frac{\partial H}{\partial q_1} = Q_1$$

$$\frac{d}{dt}\frac{\partial H}{\partial \dot{q}_2} - \frac{\partial H}{\partial q_2} = Q_2$$

$$\frac{d}{dt}\frac{\partial H}{\partial \dot{q}_3} - \frac{\partial H}{\partial q_3} = Q_3 \qquad (10)$$

$$\frac{d}{dt}\frac{\partial H}{\partial \dot{q}_4} - \frac{\partial H}{\partial q_4} = Q_4$$

The kinetic-energy will be calculated in the rotating system. Consequently the centrifugal force and the Coriolis force will be included in the generalized forces Q_n.

The kinetic energy H can be split up into two parts, the kinetic energy H_g of the gondola and the kinetic energy H_c of the cable.

The velocity has two components each one in the direction of the coordinates q_1 and q_2. For the gondola these components are

$$V_{1g} = \ell \dot{q}_1$$

$$V_{2g} = \ell \dot{q}_2$$

For a mass element of the cable having a distance x from point P the equations are:

$$V_{1c} = x \dot{q}_1$$

$$V_{2c} = x \dot{q}_2$$

Consequently

$$H = H_g + H_c = \frac{m}{2}(\mathcal{L}^2 \dot{q}_1^2 + \mathcal{L}^2 \dot{q}_2^2) + \frac{\mathcal{A}_c}{2}(\frac{\mathcal{L}^3}{3}\dot{q}_1^2 + \frac{\mathcal{L}^3}{3}\dot{q}_2^2)$$

$$+ \frac{1}{2} I_y \dot{q}_3^2 + \frac{1}{2} I_z \dot{q}_4^2 \tag{11}$$

The generalized force Q_n is the work done by the external forces during a virtual displacement δq_n divided by the displacement δq_n. The external forces are the gravitational forces, the air forces, the centrifugal forces, and the Coriolis forces, that is all forces except the cable force, which is an internal force.

The direction of the gravitational force is vertically downward. The centrifugal force is in a horizontal direction outward. The Coriolis force can be written in vector symbols

$$\bar{F}_c = -2 m \bar{\omega} \times \bar{V} \tag{12}$$

and may be split up into components according to the two components of the velocity $\bar{V}$. Since all vectors of the form $\bar{\omega} \times \bar{a}$ are perpendicular to the vector $\bar{\omega}$ which is directed vertically downward, they are all contained in a horizontal plane. The component $2\cos q_4 \mathcal{L} \omega \dot{q}_1$ points backwards, while the component $2\mathcal{L}\omega \dot{q}_2$ points away from the axis of the tower. (See Fig. 12)

The lift force L on the gondola rolls with the gondola and has almost the direction of the cable (See Fig. 12). Drag and cross forces are perpendicular to the lift.

It is assumed that the gondola is trimmed for $C_L = 0$ and $C_C = 0$ and that it moves at minimum drag coefficient as long as the speed is steady. This means that $\frac{\partial C_D}{\partial \alpha} = 0$ and $\frac{\partial C_D}{\partial \beta} = 0$.

The gondola is shown for $q_2 = 0$. Otherwise only second order terms would be added.

Fig. 12 The external forces acting on the gondola.

Subscript p means the magnitude is not shown in full value, but in projection only.
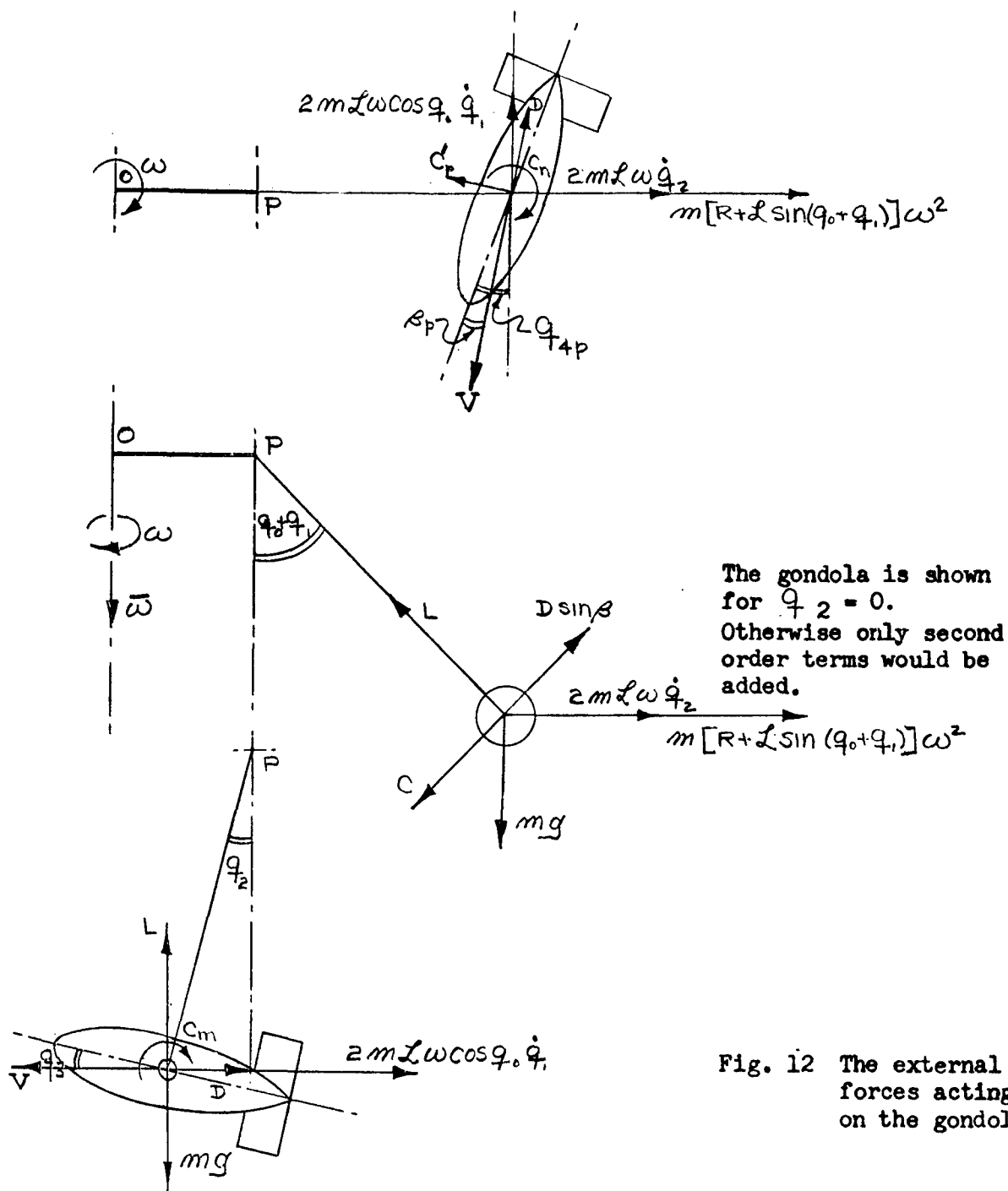
Centrifugal force: $-m\bar{\omega} \times (\bar{\omega} \times r)$

Coriolis force: $-2m\bar{\omega} \times \bar{V}$

Consequently

$$Q_1 = m\omega^2 \left[R + \ell \sin(q_o + q_1)\right] \ell \cos(q_o + q_1) - mg\ell \sin(q_o + q_1)$$

$$+ \rho_c \omega^2 \int_0^\ell \left[R + x\sin(q_o + q_1)\right] x \cos(q_o + q_1) dx - \rho g \sin(q_o + q_1)\int_0^\ell x\, dx$$

$$+ (C_D \sin\beta - C_c)\frac{\rho}{2}v^2 \otimes \ell + 2m\ell^2\omega \cos(q_o + q_1)\dot{q}_2$$

$$+ 2\rho\omega \cos(q_o + q_1)\int_0^\ell x^2 dx\, \dot{q}_2$$

or

$$Q_1 = m\left\{\omega^2\left[R + \ell\sin(q_o + q_1)\right]\ell\cos(q_o + q_1) - g\ell\sin(q_o + q_1)\right\}$$

$$+ \rho\omega^2\left[R\frac{\ell^2}{2} + \frac{\ell^3}{3}\sin(q_o + q_1)\right]\cos(q_o + q_1) - \rho\, g\sin(q_o + q_1)\frac{\ell^2}{2}$$

$$+ (C_D - \frac{\partial C_c}{\partial\beta})\beta\frac{\rho}{2}v^2\otimes\ell + 2\left[m\ell^2 + \rho\frac{\ell^3}{3}\right]\cos(q_o + q_1)\omega\dot{q}_2 \quad (13)$$

Before the generalized force Q_2 is derived, the location of the centrifugal force on the gondola relative to the virtual displacement δq_2 will be described. $\mathscr{C}$ is located in a horizontal plane and points in the direction from the axis of rotation outward (See Fig. 12). It is resolved into three components. $\mathscr{C}_{III}$ has the direction of the cable, $\mathscr{C}_I$ is perpendicular to the cable in the direction of increasing q_1, and $\mathscr{C}_{II}$ is horizontal pointing in the direction of decreasing q_2.

One reads from the rectangular spherical triangle $P'QG$ Fig. 13.

$$\cos \overgroup{P'G} = \cos q_2 \cos(q_o + q_1)$$

$$\sin q_2' = \frac{\sin q_2}{\sin \overgroup{P'G}} = \frac{\sin q_2}{\sqrt{1 - \cos^2 q_2 \cos^2(q_o + q_1)}}$$

When q_o approaches zero and if q_1 and q_2 are small one obtains for q_2' the limit value $\pi/2$ as one would expect.

For finite values of q_o and small values of q_1 and q_2 one can assume

$$q_2' = \frac{q_2}{\sqrt{1 - \cos^2 q_o}} = \frac{q_2}{\sin q_o} \quad (14)$$
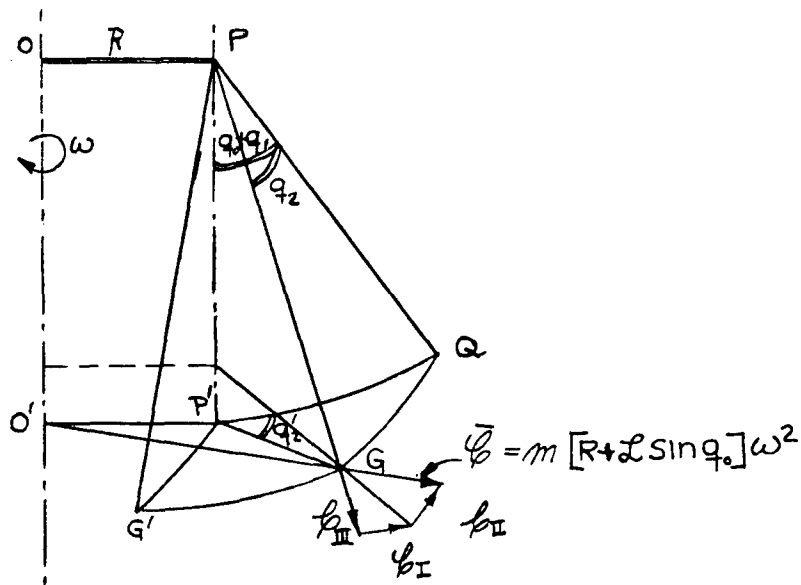
Fig. 13 Division of the centrifugal force $\bar{\mathscr{C}}$
into three components.

The location of the component $\mathscr{C}_{II}$ of the centrifugal force relative to the cable is shown in Fig. 14 in two projections.
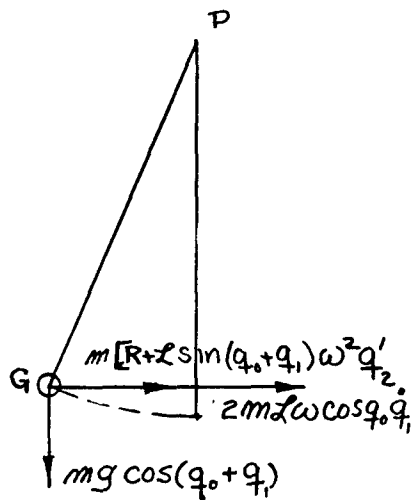
Considering that PG" is the projection of the cable length in a horizontal plane one has PG" = $\mathscr{L} \sin (q_o + q_1)$
Hence

$$\frac{R}{\mathscr{L} \sin(q_o + q_1)} = \frac{\sin \beta'}{\sin \alpha'} = \frac{\beta'}{\alpha'}$$

for small α' and β'.
Further is

$$\alpha' + \beta' = q'_2 = \frac{q_2}{\sin q_o}$$

according to equation (14).

In figure b:
$m[R + \mathscr{L} \sin(q_o + q_1)]\omega^2 q'_2$
$2m\mathscr{L}\omega \cos q_o \dot{q}_1$
$mg \cos(q_o + q_1)$

a. Plan view   b. Tangential plane

Fig. 14 Position of the centrifugal force relative to the gondola.

Hence, when q_1 is neglected in comparison to q_0:

$$\beta' = \frac{R\,q_2}{[R + \mathcal{L}\sin(q_0 + q_1)]\sin q_0} \qquad (15)$$

Using this result, the component $\mathcal{C}_{\mathrm{II}_g}$ of the centrifugal force $\mathcal{C} = m[R + \mathcal{L}\sin(q_0 + q_1)]\,\omega^2$ becomes

$$\mathcal{C}_{\mathrm{II}_g} = \mathcal{C}_g\,\beta' = \frac{m\,R\,\omega^2}{\sin q_0} \cdot q_2$$

This force is perpendicular to PG". Similarly one obtains for the corresponding component of the centrifugal force on a cable element

$$d\,\mathcal{C}_{\mathrm{II}_c} = \frac{\rho\,R\,\omega^2\,dx}{\sin q_0} \cdot q_2$$

After adding the contribution of gravitation, of the Coriolis force, and of the air forces one obtains the generalized force

$$Q_2 = -\left\{ g\cos(q_0 + q_1)\left[m\mathcal{L} + \rho\frac{\mathcal{L}^2}{2}\right] + \frac{m + \rho\frac{\mathcal{L}}{2}}{\sin q_0}\,R\,\mathcal{L}\,\omega^2 \right\} q_2$$
$$- 2\,\dot{q}_1\,\mathcal{L}^2\,\omega\cos q_0\,\left(m + \rho\frac{\mathcal{L}}{3}\right) - D\mathcal{L} \qquad (16)$$

This equation is not valid for $q_0 = 0$, since equation (14) has been used. The case $q_0 = 0$, however, is of no interest. The contribution of the lift force is but small and of second order and has been neglected.

The Coriolis force might be treated in the same way as the centrifugal force. Since, however, the Coriolis force is small but of the first order, the moment which originates from it by the multiplication by q_2 would be small and of the second order. This component is therefore neglected. The generalized forces Q_3 and Q_4 include aerodynamic moments only.

$$Q_3 = \left(\frac{\partial C_m}{\partial \alpha}\,\alpha + \frac{\partial C_m}{\partial \dot{q}_3}\,\dot{q}_3\right) \otimes l\,\frac{\rho}{2}\,V^2 \qquad (17)$$

$$Q_4 = \left(\frac{\partial C_n}{\partial \beta}\,\beta + \frac{\partial C_n}{\partial \dot{q}_4}\,\dot{q}_4\right) \otimes l\,\frac{\rho}{2}\,V^2 \qquad (18)$$

The mass forces do not contribute to the moments Q_3 and Q_4 since Q_3 and Q_4 are rotations about the center of gravity. When the values (17) and (18) are substituted into the equations of motion it will be considered that

$$\alpha = q_3 \tag{19}$$

$$\beta = q_4 + \frac{\mathcal{L}\,\dot{q}_1}{(R + \mathcal{L}\sin q_o)\omega} \tag{20}$$

These values are now substituted into the Lagrangian equations of motion (10).

$$\frac{d}{dt}\frac{\partial H}{\partial \dot{q}_1} = \left(m\mathcal{L}^2 + \mathcal{P}\frac{\mathcal{L}^3}{3}\right)\ddot{q}_1 \qquad\qquad \frac{d}{dt}\frac{\partial H}{\partial \dot{q}_3} = I_y\,\ddot{q}_3$$

$$\frac{\partial H}{\partial q_1} = 0 \qquad\qquad\qquad \frac{\partial H}{\partial q_3} = 0$$

$$\frac{d}{dt}\frac{\partial H}{\partial \dot{q}_2} = \mathcal{L}^2\left(m + \frac{\mathcal{L}}{3}\mathcal{P}\right)\ddot{q}_2 \qquad\qquad \frac{d}{dt}\frac{\partial H}{\partial \dot{q}_4} = I_z\,\ddot{q}_4$$

$$\frac{\partial H}{\partial q_2} = 0 \qquad\qquad\qquad \frac{\partial H}{\partial q_4} = 0$$

Consequently the equations of motion are:

$$\left(m + \mathcal{P}\frac{\mathcal{L}}{3}\right)\mathcal{L}^2\ddot{q}_1 =$$

$$m\left\{\left[R + \mathcal{L}\sin(q_o + q_1)\right]\mathcal{L}\cos(q_o + q_1)\omega^2 - g\mathcal{L}\sin(q_o + q_1) + 2\mathcal{L}^2\omega\cos(q_o + q_1)\dot{q}_2\right\}$$

$$+ \mathcal{P}\left\{\left[R\frac{\mathcal{L}}{2} + \frac{\mathcal{L}^3}{3}\sin(q_o + q_1)\right]\omega^2\cos(q_o + q_1) - g\frac{\mathcal{L}^2}{2}\sin(q_o + q_1) + 2\frac{\mathcal{L}^3}{3}\omega\cos(q_o + q_1)\dot{q}_2\right\}$$

$$+ \left(C_D - \frac{\partial C_L}{\partial \beta}\right)\frac{\mathcal{P}}{2}V^2 \otimes \mathcal{L}\left(q_4 + \frac{\mathcal{L}\dot{q}_1}{(R + \mathcal{L}\sin q_o)\omega}\right)$$

$$\tag{21}$$

$$(m + \tfrac{\mathscr{L}}{3}\rho)\,\mathscr{L}^2\ddot{q}_2 + 2(m + \rho\tfrac{\mathscr{L}}{3})\mathscr{L}^2\omega\dot{q}_1\cos q_0$$

$$+ \left\{ g\cos(q_0+q_1)\left[m\mathscr{L} + \rho\tfrac{\mathscr{L}^2}{2}\right] + \frac{m+\rho\tfrac{\mathscr{L}}{2}}{\sin q_0}R\mathscr{L}\omega^2\right\}q_2$$

$$+ \frac{\rho}{2}V^2 C_D \otimes \mathscr{L} = 0 \qquad\qquad (22)$$

$$I_y\ddot{q}_3 - \left[\frac{\partial C_m}{\partial\alpha}q_3 + \frac{\partial C_m}{\partial\dot{q}_3}\dot{q}_3\right]\otimes l\frac{\rho}{2}V^2 = 0 \qquad (23)$$

$$I_z\ddot{q}_4 - \left[\frac{\partial C_n}{\partial\beta}\left(q_4 + \frac{\mathscr{L}\dot{q}_1}{(R+\mathscr{L}\sin q_0)\omega}\right) + \frac{\partial C_n}{\partial\dot{q}_4}\dot{q}_4\right]\otimes l\frac{\rho}{2}V^2 = 0 \qquad (24)$$

Linearization and Nondimensionalization

of the Equations of Motion

The investigation will be confined to small disturbances to the steady motion. Therefore it is permissible to neglect terms which are proportional to quadratic and higher powers of the disturbances. If the angle, by which the gondola lags the whirling arm, is disregarded, the disturbances are q_1, q_2, q_3, and q_4. Terms, which do not include these variables belong to the steady state motion, which has already been taken care of. Consequently only those terms are retained in the equations of motion which are linear in q_1, q_2, q_3, and q_4.

If one uses the abbreviation:

$$V_0 = (R + \mathscr{L}\sin q_0)\omega$$

the square of the speed can be linearized as follows:

$$V^2 = V_0^2 + 2\mathscr{L}\left[R + \mathscr{L}\sin q_0\right]\left[\cos q_0\,\omega^2 q_1 + \omega\dot{q}_2\right] \qquad (25)$$

After linearization one obtains from equations (21) to (24)

$$(m + \rho\tfrac{\mathscr{L}}{3})\mathscr{L}^2\ddot{q}_1 =$$

$$m\left\{-\left[R+\mathscr{L}\sin q_0\right]\mathscr{L}\omega^2\sin q_0 q_1 + \mathscr{L}^2\cos^2 q_0\,\omega^2 q_1 - g\mathscr{L}\cos q_0 q_1 + 2\mathscr{L}^2\cos q_0\,\omega\dot{q}_2\right\}$$

$$+ \rho\left\{-\left[\tfrac{R}{2}+\tfrac{\mathscr{L}}{3}\sin q_0\right]\mathscr{L}^2\omega^2\sin q_0 q_1 + \tfrac{\mathscr{L}^3}{3}\cos^2 q_0\,\omega^2 q_1 - g\tfrac{\mathscr{L}^2}{2}\cos q_0 q_1 + 2\tfrac{\mathscr{L}^3}{3}\cos q_0\,\omega\dot{q}_2\right\} \qquad (26)$$

$$+ \left(C_D - \frac{\partial C_L}{\partial\beta}\right)\left[q_4 + \frac{\mathscr{L}\dot{q}_1}{(R+\mathscr{L}\sin q_0)\omega}\right]\frac{\rho}{2}V_0^2 \otimes \mathscr{L}$$

$$\left(m+\tfrac{\mathcal{L}}{3}\right)\mathcal{L}^2\ddot{q}_2 + 2\left(m+\mathcal{L}\tfrac{\mathcal{L}}{3}\right)\mathcal{L}^2\omega\dot{q}_1\cos q_0$$

$$+ \left\{g\cos q_0\left(m\mathcal{L}+\mathcal{L}\tfrac{\mathcal{L}^2}{2}\right) + \tfrac{m+\mathcal{L}\frac{\mathcal{L}}{2}}{\sin q_0}R\mathcal{L}\,\omega^2\right\}q_2$$

$$+\rho\mathcal{L}^2(R+\mathcal{L}\sin q_0)(\cos q_0\,\omega^2 q_1 + \omega\dot{q}_2)\,C_D\otimes\mathcal{L} = 0 \tag{27}$$

$$I_y\ddot{q}_3 - \left(\tfrac{\partial C_m}{\partial\alpha}q_3 + \tfrac{\partial C_m}{\partial\dot{q}_3}\dot{q}_3\right)\otimes\mathcal{L}\tfrac{\rho}{2}V_0^2 = 0 \tag{28}$$

$$I_z\ddot{q}_4 - \left[\tfrac{\partial C_m}{\partial\beta}\left(q_4 + \tfrac{\mathcal{L}\dot{q}_1}{(R+\mathcal{L}\sin q_0)\omega}\right) + \tfrac{\partial C_m}{\partial\dot{q}_4}\dot{q}_4\right]\otimes\mathcal{L}\tfrac{\rho}{2}V_0^2 = 0 \tag{29}$$

These equations will be transformed into the nondimensional form. The nondimensional form has the advantage of a direct comparison between full scale and model tests and making clear which combinations of the parameters are essential. Moreover, the coefficients of the equations become all of the same order of magnitude which makes it more convenient to handle.

For this purpose, the following substitutions are made: Instead of seconds, the value τ is used as a unit of time, which is defined by:

$$\tau = \frac{m}{\rho\otimes V_0} \qquad [\text{SEC.}] \tag{30}$$

The mass factor:

$$\mu = \frac{m}{\rho\otimes\mathcal{L}} \tag{31}$$

and the following abbreviations are introduced

$$\overline{\omega} = \omega\tau \qquad\qquad k_y^2 = \frac{1}{\mu}\frac{I_y}{m\mathcal{L}^2}$$

$$\overline{g} = \frac{g}{\mathcal{L}}\tau^2 \qquad\qquad k_z^2 = \frac{1}{\mu}\frac{I_z}{m\mathcal{L}^2} \tag{32}$$

$$\overline{R} = \frac{R\mathcal{L}}{m}$$

$$\overline{t} = \frac{t}{\tau} \qquad\qquad M = 1+\frac{\overline{R}}{3} = 1+\frac{\mathcal{L}\mathcal{L}}{3m}$$

28

Primes ($'$) are used for designating derivatives with respect to $\bar{t}$.

After multiplying equations (26) and (27) with $\dfrac{\tau^2}{m\mathcal{L}^2}$ and after dividing equations (28) and (29) with $\rho V_o^2 \otimes \mathcal{L}$ one obtains

$$M q_1'' + (\tfrac{R}{\mathcal{L}} + \sin q_o)\bar{\omega}^2 \sin q_o q_1 - \cos^2 q_o \bar{\omega}^2 q_1 + \bar{g}\cos q_o q_1 - 2\cos q_o \bar{\omega} q_2'$$
$$+ \mathcal{A}\left[(\tfrac{1}{2}\tfrac{R}{\mathcal{L}} + \tfrac{1}{3}\sin q_o)\bar{\omega}^2 \sin q_o q_1 - \tfrac{1}{3}\cos^2 q_o \bar{\omega}^2 q_1 + \tfrac{\bar{g}}{2}\cos q_o q_1 - \tfrac{2}{3}\cos q_o \bar{\omega} q_2'\right\}$$
$$- \tfrac{1}{2}\tfrac{\mathcal{l}}{\mathcal{L}}\mu(C_D - \tfrac{\partial C_c}{\partial \beta})(q_4 + \frac{\mathcal{L}}{(R + \mathcal{L}\sin q_o)\bar{\omega}} q_1') = 0 \qquad (33)$$

$$M q_2'' + 2M\bar{\omega} q_1' \cos q_o$$
$$+ \left\{\bar{g}\cos q_o(1 + \tfrac{\mathcal{A}\mathcal{L}}{2m}) + \frac{1 + \tfrac{\mathcal{A}\mathcal{L}}{2m}}{\sin q_o}\tfrac{R}{\mathcal{L}}\bar{\omega}^2\right\}q_2$$
$$+ \tfrac{1}{\mu}(\tfrac{R}{\mathcal{l}} + \tfrac{\mathcal{L}}{\mathcal{l}}\sin q_o)(\cos q_o \bar{\omega}^2 q_1 + \bar{\omega} q_2') C_D = 0 \qquad (34)$$

$$\mathcal{k}_y^2 q_3'' - \tfrac{1}{2}\left(\frac{\partial C_m}{\partial \alpha} q_3 + \frac{\partial C_m}{\partial q_3'} q_3'\right) = 0 \qquad (35)$$

$$\mathcal{k}_z^2 q_4'' - \tfrac{1}{2}\left[\frac{\partial C_n}{\partial \beta}(q_4 + \frac{\mathcal{L} q_1'}{(R + \mathcal{L}\sin q_o)\bar{\omega}}) + \frac{\partial C_n}{\partial q_4'} q_4'\right] = 0 \qquad (36)$$

After collecting terms the following equations are obtained:

$$M q_1'' - \tfrac{1}{2}\mu(C_D - \tfrac{\partial C_c}{\partial \beta})\frac{\mathcal{l}}{(R + \mathcal{L}\sin q_o)\bar{\omega}} q_1'$$
$$+ \left\{[\tfrac{R}{\mathcal{L}} + \sin q_o + \tfrac{\mathcal{A}}{2}(\tfrac{R}{\mathcal{L}} + \tfrac{2}{3}\sin q_o)]\bar{\omega}^2 \sin q_o - \bar{\omega}^2 \cos^2 q_o\right.$$
$$+ \mathcal{A}(\tfrac{\bar{g}}{2} - \tfrac{1}{3}\bar{\omega}^2 \cos q_o)\cos q_o + \bar{g}\cos q_o\right\}q_1$$
$$- 2M\cos q_o \bar{\omega} q_2' - \tfrac{1}{2}\tfrac{\mathcal{l}}{\mathcal{L}}\mu(C_D - \tfrac{\partial C_c}{\partial \beta})q_4 = 0 \qquad (38)$$

$$2\cos q_o M\bar{\omega} q_1' + \tfrac{1}{\mu}(\tfrac{R}{\mathcal{l}} + \tfrac{\mathcal{L}}{\mathcal{l}}\sin q_o)\cos q_o \bar{\omega}^2 C_D q_1 \qquad (39)$$
$$+ M q_2'' + \tfrac{1}{\mu}(\tfrac{R}{\mathcal{l}} + \tfrac{\mathcal{L}}{\mathcal{l}}\sin q_o)\bar{\omega} C_D q_2'$$
$$+ \left\{(\bar{g}\cos q_o + \frac{R}{\mathcal{L}\sin q_o}\bar{\omega}^2)(1 + \tfrac{\mathcal{A}}{2})\right\}q_2 = 0$$

$$k_y^2 q_3'' - \frac{1}{2}\frac{\partial C_m}{\partial q_3'} q_3' - \frac{1}{2}\frac{\partial C_m}{\partial \alpha} q_3 \qquad = 0 \qquad (40)$$

$$-\frac{1}{2}\frac{\partial C_n}{\partial \beta}\frac{\ell}{(R+\mathcal{L}\sin q_0)\overline{\omega}} q_1' + k_z^2 q_4'' - \frac{1}{2}\frac{\partial C_n}{\partial q_4} - \frac{1}{2}\frac{\partial C_n}{\partial \beta} q_4 = 0 \qquad (41)$$

The solution of the equations is assumed in the form

$$q_n = A_n e^{\nu_n \frac{t}{\mathcal{E}}} = A_n e^{(-\zeta_n + \omega_n)\frac{t}{\mathcal{E}}} \qquad (42)$$

If the solution is not identically zero, which would represent the case of undisturbed motion, which is of no interest here, the determinant of the system of equations (38) to (41) must vanish. This determinant has the form

$$(43) \quad \begin{vmatrix} c_{11}\nu^2 + b_{11}\nu + a_{11} & b_{12}\nu & \underline{\qquad} & a_{44} \\ b_{21}\nu + a_{21} & c_{22}\nu^2 + b_{22}\nu + a_{22} & \underline{\qquad} & \underline{\quad}\underline{\quad} \\ \underline{\qquad} & \underline{\qquad} & c_{33}\nu^2 + b_{33}\nu + a_{33} & \underline{\quad}\underline{\quad} \\ b_{41}\nu & \underline{\qquad} & \underline{\qquad} & c_{44}\nu^2 + b_{44}\nu + a_{44} \end{vmatrix} = 0$$

where

$$c_{11} = c_{22} = M$$

$$b_{11} = -\frac{1}{2}\mu\left(C_D - \frac{\partial C_L}{\partial \beta}\right)\frac{\ell}{(R+\mathcal{L}\sin q_0)\overline{\omega}} = -\frac{1}{2}\left(C_D - \frac{\partial C_L}{\partial \beta}\right)$$

$$a_{11} = \left[\frac{R}{\mathcal{L}}\left(1+\frac{\overline{\mathcal{L}}}{2}\right)+M\sin q_0\right]\overline{\omega}^2\sin q_0 - \overline{\omega}^2 M\cos^2 q_0 + \overline{g}\left(1+\frac{\overline{\mathcal{L}}}{2}\right)\cos q_0$$

$$b_{12} = -2M\overline{\omega}\cos q_0$$

$$a_{14} = -\frac{1}{2}\frac{\ell}{\mathcal{L}}\mu\left(C_D - \frac{\partial C_L}{\partial \beta}\right) \qquad (44)$$

$$b_{21} = 2M\overline{\omega}\cos q_0 = -b_{12}$$

$$a_{21} = \frac{1}{\mu}\left(\frac{R}{\mathcal{L}}+\frac{\mathcal{L}}{\mathcal{L}}\sin q_0\right)\cos q_0 \,\overline{\omega}^2 C_D = \overline{\omega}\, C_D \cos q_0$$

$$b_{22} = \frac{1}{\mu}\left(\frac{R}{l} + \frac{l}{l}\sin q_0\right)\bar{\omega}\, C_D = C_D$$

$$a_{22} = \left(\bar{g}\cos q_0 + \frac{R}{l\sin q_0}\bar{\omega}^2\right)\left(1 + \frac{\bar{l}}{2}\right)$$

$$C_{33} = k_y^2$$

$$b_{33} = -\frac{1}{2}\frac{\partial C_m}{\partial q_3'}$$

$$a_{33} = -\frac{1}{2}\frac{\partial C_m}{\partial \alpha}$$

$$b_{41} = -\frac{1}{2}\frac{\partial C_n}{\partial \beta}\frac{l}{(R+l\sin q_0)\bar{\omega}}$$

$$C_{44} = k_z^2$$

$$b_{44} = -\frac{1}{2}\frac{\partial C_n}{\partial q_4'}$$

$$a_{44} = -\frac{1}{2}\frac{\partial C_n}{\partial \beta}$$

$$(44)$$

It follows from the determinant (43) that the pendulum degrees of freedom q_1 and q_2 are independent from the rotary degrees of freedom q_3 and q_4 if either a_{14} or b_{41} is zero. a_{14} can become exactly zero, if $C_D = \frac{\partial C_c}{\partial \beta}$, although even a slight deviation from the exact zero gives a_{14} an appreciable value because of the large numerical value of μ with which $(C_D - \frac{\partial C_c}{\partial \beta})$ is multiplied.

The other condition under which the separation of the two groups would take place is that

$$b_{41} = -\frac{1}{2}\frac{\partial C_n}{\partial \beta}\frac{l}{(R+l\sin q_0)\bar{\omega}}$$

would be negligibly small. Since $\frac{l}{(R+l\sin q_0)\bar{\omega}}$ is of the order of .02 and since $C_n(\beta)$ is very likely to have a S type characteristic with an almost horizontal tangent for $\beta = 0$, $\frac{\partial C_n}{\partial \beta}$ would also be very small.

Therefore the assumption that $b_{41} = 0$ is a good approximation. Nevertheless it should be kept in mind, that from here on the investigation is somewhat simplified.

If $b_{41} = 0$, the determinant (43) splits up into

$$(C_{33}\nu^2 + b_{33}\nu + a_{33})(C_{44}\nu^2 + b_{44}\nu + a_{44})\begin{vmatrix} C_{11}\nu^2 + b_{11}\nu + a_{11} & b_{12}\nu \\ b_{21}\nu + a_{21} & C_{22}\nu^2 + b_{22}\nu + a_{22} \end{vmatrix} = 0 \quad (45)$$

Instead of an eigth degree polynominal, two quadratic and one quartic equation has to be investigated.

Stability of the Coupled Pendulum Degrees of Freedom

The quartic determining the stability of the pendulum degrees of freedom q_1 and q_2 can be written:

$$A_4 v^4 + A_3 v^3 + A_2 v^2 + A_1 v + A_o = 0 \qquad (46)$$

Here, the following abbreviations are used:

$$A_4 = C_{11} \, C_{22}$$

$$A_3 = C_{11} \, b_{22} + C_{22} \, b_{11}$$

$$A_2 = C_{11} \, a_{22} + b_{11} \, b_{22} + C_{22} \, a_{11} - b_{21} \, b_{12} \qquad (47)$$

$$A_1 = b_{11} \, a_{22} + b_{22} \, a_{11} - b_{12} \, a_{21}$$

$$A_o = a_{11} \, a_{22}$$

The conditions for stability are

$$A_4 > 0; \quad A_3 > 0; \quad A_2 > 0; \quad A_1 > 0; \quad A_0 > 0$$
$$R = A_1 A_2 A_3 - A_1^2 A_4 - A_o A_3^2 > 0$$

If the Routhian discriminant, R, is going to be chosen as a measure of stability, the coefficient A_4 of the frequency polynomial must be made equal to one. This means that each coefficient A is divided by $A_4 = M^2$. If we retain the coefficients as being given by equations (47), the discriminant Routhian has to be divided by M^6. One has

$$\frac{R}{M^6} = \frac{1}{M^6} \left[A_1 (A_2 A_3 - A_1 A_4) - A_o A_3^2 \right]$$

Substituting the values from equations (47) and (44) and considering that $b_{11} = 0$ one obtains:

$$A_2 A_3 - A_1 A_4 = C_D M^2 (\alpha_{11} + \alpha_{22} + 4M \bar{\omega}^2 \cos^2 q_o) - M^2 (C_D \alpha_{11} + 2M \bar{\omega}^2 \cos^2 q_o C_D)$$

$$= C_D M^2 \left\{ \alpha_{22} + 2M \bar{\omega}^2 \cos^2 q_o \right\}$$

$$A_1 (A_2 A_3 - A_1 A_4) = C_D^2 M^2 (\alpha_{11} + 2M \bar{\omega}^2 \cos^2 q_o)(\alpha_{22} + 2M \bar{\omega}^2 \cos^2 q_o)$$

$$A_0 A_3^2 = a_{11} a_{22} M^2 C_D^2$$

$$\frac{R}{M^6} = \frac{C_D^2}{M^4}\left\{(a_{11}+a_{22})\,2\,M\,\bar{\omega}^2\cos^2 q_0 + 4 M^2 \bar{\omega}^4 \cos^4 q_0\right\}$$

$$\frac{R}{M^6} = \frac{2 C_D^2}{M^3}\,\bar{\omega}^2\cos^2 q_0\left\{a_{11}+a_{22}+2\,M\,\bar{\omega}^2\cos^2 q_0\right\}$$

The values of a_{11} and a_{22} are also substituted according to equations (44). The abbreviation

$$N = \frac{1+\frac{\bar{R}_c}{2}}{1+\frac{\bar{R}_c}{3}} = \frac{1+\frac{\bar{R}_c}{2}}{M} \tag{48}$$

is used. It is

$$a_{11} = M\left\{\frac{R}{\mathcal{L}}\,N\,\bar{\omega}^2\sin q_0 + \bar{\omega}^2(\sin^2 q_0 - \cos^2 q_0) + \bar{g}\,N\cos q_0\right\}$$

$$a_{22} = MN\left\{\bar{g}\cos q_0 + \frac{R}{\mathcal{L}\sin q_0}\,\bar{\omega}^2\right\}$$

Hence

$$\frac{R}{M^6} = \frac{2 C_D^2}{M^2}\,\omega^4\cos^2 q_0\left\{1 + N\left[\frac{2\bar{g}}{\bar{\omega}^2}\cos q_0 + \frac{R}{\mathcal{L}}\left(\sin q_0 + \frac{1}{\sin q_0}\right)\right]\right\}$$

After substituting the nondimensional values $\bar{g}$ and $\bar{\omega}$ by the original values one obtains

$$\frac{R}{M^6} = \frac{2 C_D^2\cos^2 q_0\, m^4}{\rho^4 \otimes^4 (R+\mathcal{L}\sin q_0)^4 M^2}\left\{1 + N\left[\frac{2g}{\mathcal{L}\omega^2}\cos q_0 + \frac{R}{\mathcal{L}}\left(\sin q_0 + \frac{1}{\sin q_0}\right)\right]\right\} \tag{49}$$

Since $0 \leq q_0 \leq \frac{\pi}{2}$ it is obvious that $\frac{R}{M^6}$ can never become negative. Consequently the only possibility of $\frac{R}{M^6}$ instability is that one of the coefficients A_n may become negative. Numerical calculations will show, however, that this is not the case. Consequently no dynamic instabilities are to be expected.

The result of a numerical investigation of the stability of the system with a single torsion free cable is reproduced in Table III. The calculations are based on the data of Table I. The calculations are made for the fully loaded gondola of W = 685 lbs and for a cable with a weight of 5.17 lb/ft including the weight of the sheathing.

The Table III lists the coefficients A_0, A_1, and A_2 of the frequency polynomial for the range of q_o from 5° to 85°. A_3 and A_4 have the constant values $A_3 = .2326$; $A_4 = 1.670$. The drag coefficient of the gondola including part of the cable drag is assumed to be $C_D = 0.24$. This value might actually be somewhat higher. This difference, however, would affect the stability only very slightly.

The frequency polynomial has been solved by means of the method developed by H. C. Gebelein* which is considered especially suited for cases like the present one, where the roots are located relatively close to each other. The damping ratios ζ_1 and ζ_2 are extremely low, i.e., in the order of about 10^{-7} and 10^{-3}. Because of equation (49), however, one is sure that an inaccurate assumption or a variation of the data will not lead to instability.

The periods T_1 and T_2, which were calculated previously neglecting the mutual couplings, are also listed in Table III. A comparison with the former values shows that the coupling decreases the periods at all cable angles q_o. The cable angle, however, for which the two periods are equal to each other, remains the same (52.4°).

MODEL TESTS

The theoretical investigations shown on the preceding pages had to be made without reference to other reports since no analytical treatment of the same or a similar problem was known. Therefore it was desirable to verify the results by tests at least qualitatively.

Checks on the full scale equipment were out of the question because of required time and cost. Therefore recourse was made to tests on a 1:20 scale model.

It is obvious that a dynamically similar model in an exact sense could not be built. While, for instance, the full scale Reynolds number of the round unsheathed cable is above the critical number, the corresponding Reynolds number of the model was below the critical number.

These insufficiencies, however, were not considered serious, since the theory had revealed their secondary importance. The intent of the model tests was not so much to reproduce the characteristics of the full scale equipment as to check qualitative theoretical results similar to the following. The frequency of the two pendulum modes is about equal and as long as the cable angle is below 70° both periods are shorter than

* H. C. Gebelein: Treatment of Fourth Degree Equations - AF Tech Rpt No. 5992.

the period of turning of the arm. All configurations going to be tested will be stable, but the damping will be very low.

It was especially the latter result which would represent a sensitive check. The only instrumentation needed would be some means of recording the motion following a disturbance.

Dynamic Similarity

The dynamic similarity of the model was based on the length scale factor $\Lambda = 1{:}20$ and on the requirement that the direction of the resultant of centrifugal and gravitational forces should be the same for the model and for the full scale equipment. Since the gravitational acceleration g is the same for model and full scale equipment, the centrifugal acceleration $\frac{V^2}{r}$ had also to be the same. This means that the circumferential speeds had to have the ratio $V_{model} : V_{full\ scale} = 1 : \sqrt{20}$

Masses were reduced by the factor $\Lambda^3 = 1{:}8000$. This applies to the mass of the gondola and of the cable. The similarity of the air forces is fulfilled automatically.

For two reasons, no effort was made to obtain similarity of the moments of inertia of the gondola. First, the moment of the inertia of the present gondola was not known and the data on the new gondola which is going to be designed were not yet available. Secondly, the theoretical investigations had shown that there would be very little coupling between the rotational degrees of freedom and the pendulum degrees of freedom which are of interest here.

Model Test Equipment

It was out of the question to build more than one gondola model. Since the full scale gondola will later on be suspended with a single cable attached above the center of gravity, the single cable suspension was reproduced by the model. The dimensions of the new gondola were not yet available. Therefore the model was built in the form of the old gondola adapted to a single point suspension as being used at El Centro by that time. The cable was attached to a yoke, which connects the two former point of attachments (See Fig. 15 and 16).

This arrangement has a large lateral area. Therefore the condition $C_D - \frac{\partial C_c}{\partial \beta} = 0$ was very likely not fulfilled. Hence it was expected that tests with this model would also indicate to what degree a violation of the assumption $C_D - \frac{\partial C_c}{\partial \beta} = 0$ would modify the theoretical results.

YOKE CONVERTING TWO POINT SUSPENSION INTO SINGLE POINT SUSPENSION.
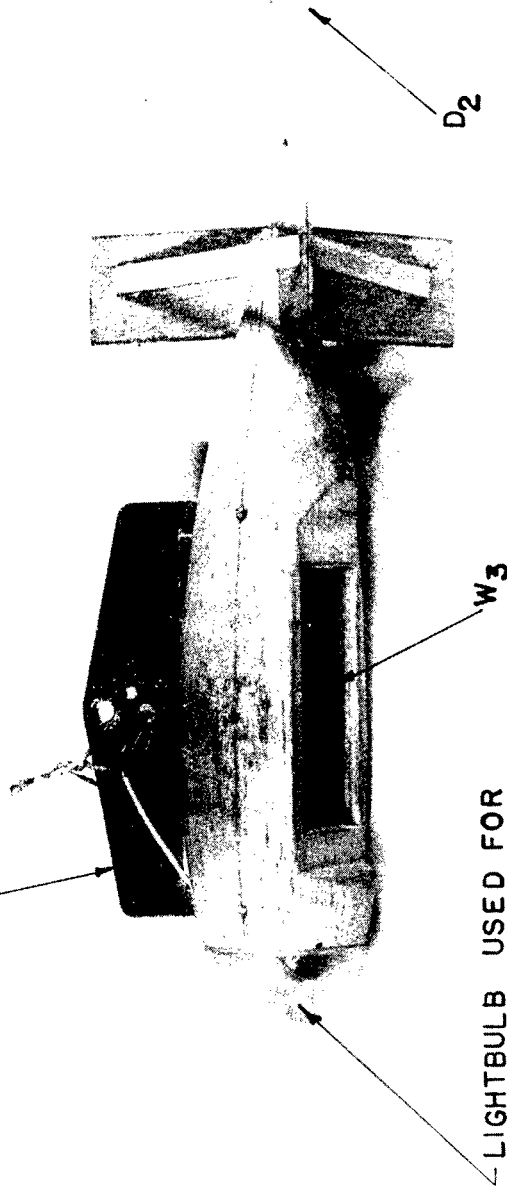
LIGHTBULB USED FOR RECORDING OF MOTION

W_3

D_2

Fig. 15   Gondola With Heaviest Weight, W_3, and
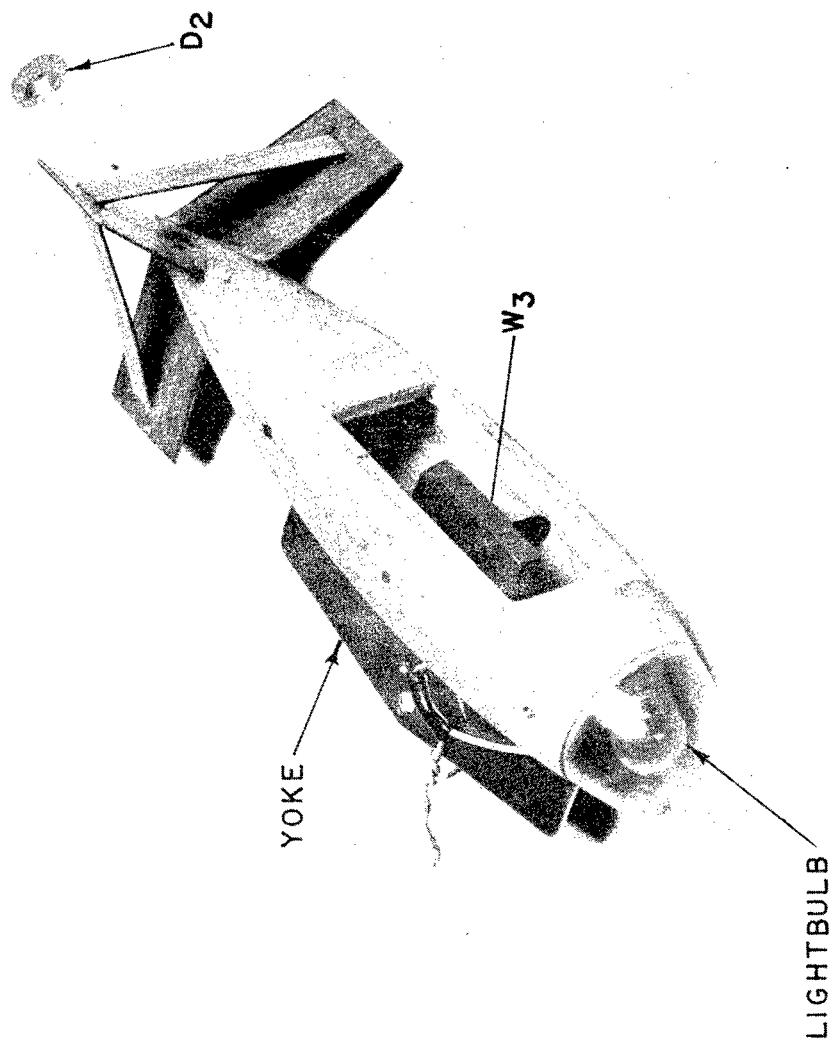
Medium Drag Plate, D_2

Fig. 16   Gondola With Heaviest Weight, W_3, and
          Medium Drag Plate, D_2

The driving mechanism consisted, during the first tests, of an electric motor designed for high gondola speeds. At the test speeds, which were much lower, the motion was erratic. Even when a gear reduction of 11:1 was used the motion was not even enough for reliable measurement.

Therefore, the electric motor was replaced by a compressed air motor. Though this gave a much smoother drive serious fluctuations of the speed were encountered when other tools connected with the same compressed air tank were in operation. The available pressure regulator could not cope with these pressure fluctuations. Finally an electric motor controlled by the Ward Leonard system was installed, which gave satisfactory smoothness of the turning speed. (Fig. 17)

The disturbance of the motion was produced by a jet of compressed air. The jet was formed by a nozzle mounted on a tripod (Fig. 18). A suitable direction of the nozzle was found by trial before a measurement was made. The distance of the nozzle from the gondola path was so chosen that the disturbance was of a reasonable magnitude.

The purpose of the tests was to obtain numerical results on the periods and the dampings of the disturbed gondola motion. The easiest way was considered to be the taking of time exposure pictures of the motion. For this purpose, the nose of the gondola was made of transparent plastic and an electric light bulb was installed underneath of the plastic cover (See Fig. 15 and 16). Light bulbs were also mounted on the end of the turning arm and at the turning center (Fig. 18). The traces of these two latter light bulbs helped in aligning and comparing photographs of different tests.

Two cameras of 4" x 5" size were used for recording the motion. One camera was located above the model tower. By means of a plumb line the optical axis of the camera was lined up with the axis of rotation. The view taken by this camera is shown in Fig. 20. The other camera was on a tripod facing the model tower. The distance of its lens from the axis of rotation was 29 feet, 2-1/2 inches. Its optical axis had the same height above the floor as the turning arm. A view taken by this camera is given by Fig. 21.

Eighteen different test combinations of gondola weight, cable weight and additional drag were tested, as listed in the following table.

Run No.	Gondola Weight	Cable No.	Gondola Drag
1	W_1	C_1	D_1
2	W_2	C_1	D_1
3	W_3	C_1	D_1

CENTER BULB

DRY CELLS

WHIRL ARM

FLEXIBLE SHAFT
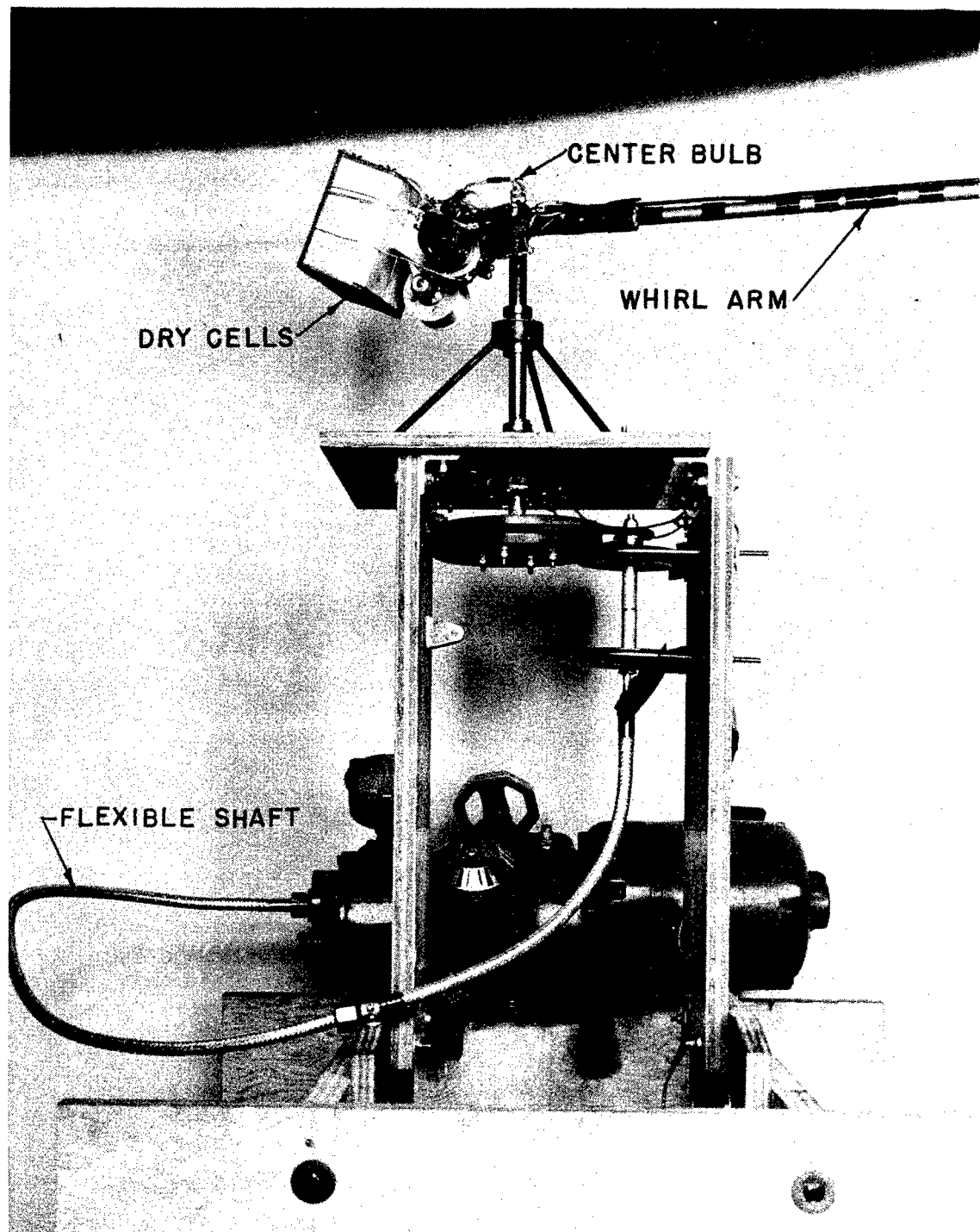
Fig. 17   The Driving Mechanism

Fig. 18   Model Set-Up Showing Application

Of Disturbance

PROTRACTOR USED
FOR SPEED ADJUST-
-MENT
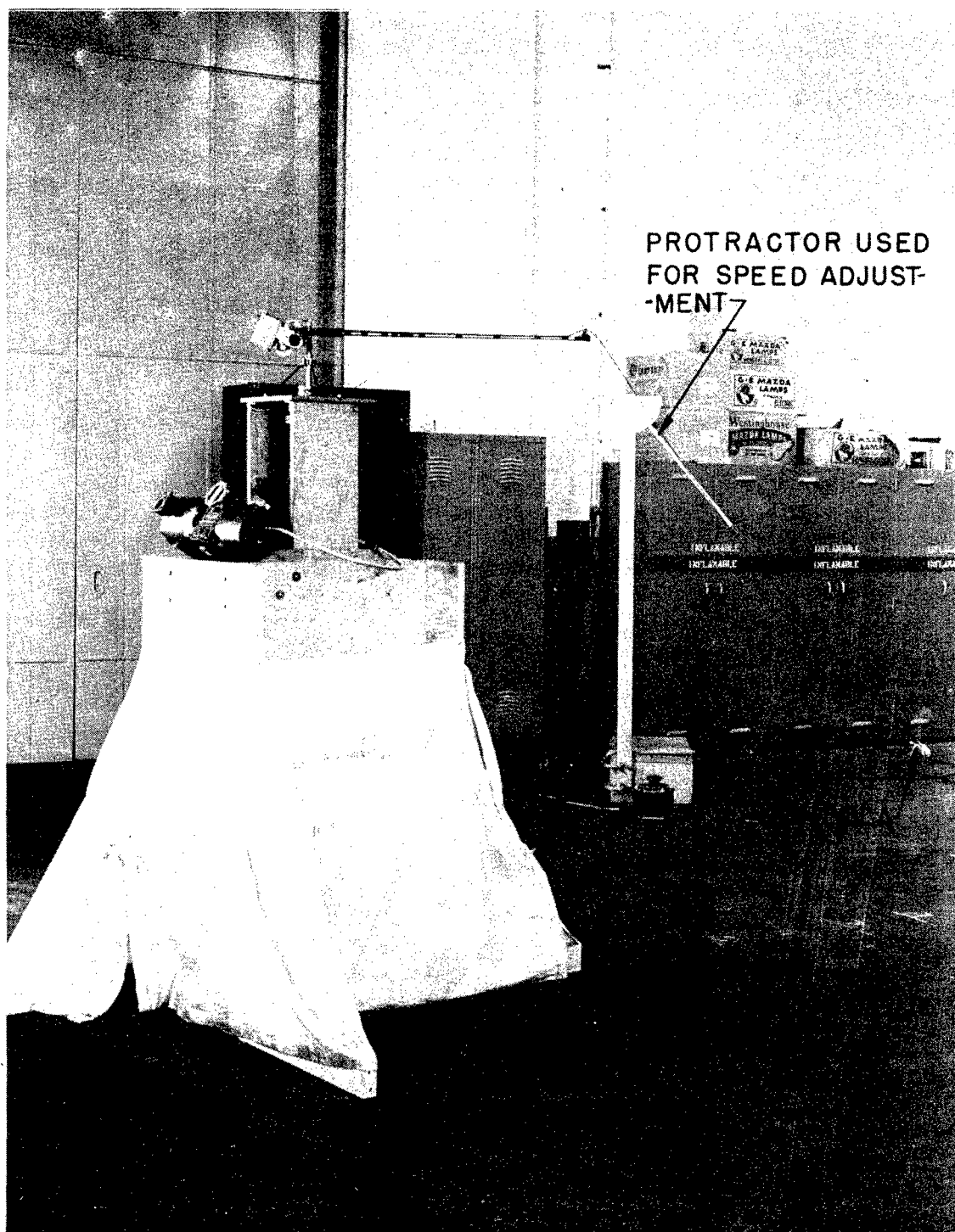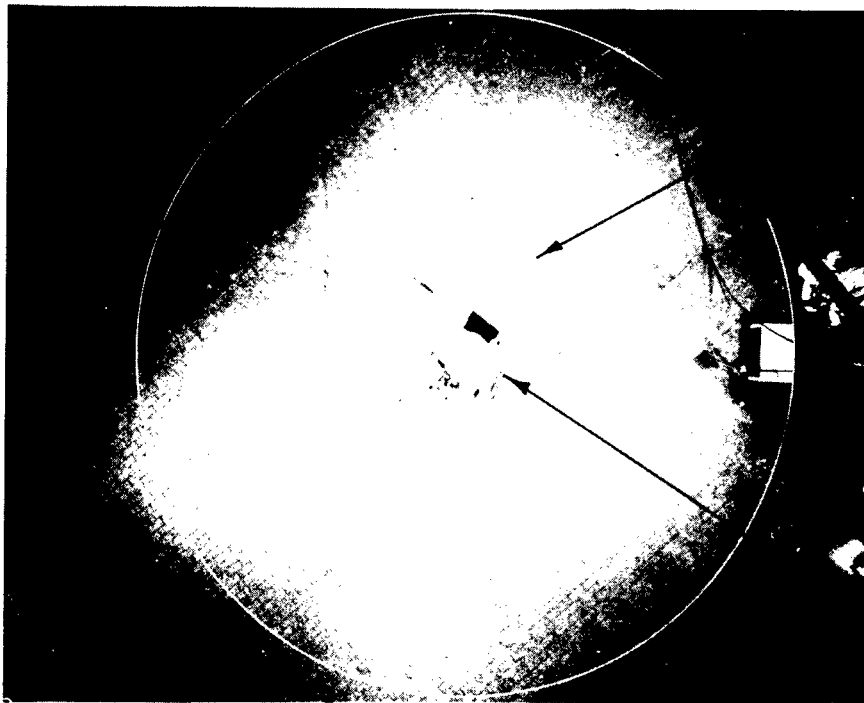
Fig. 19 Model Set-Up Showing Use

Of Protractor For Speed Adjustment

-Trace of
Tip Bulb

-Trace of
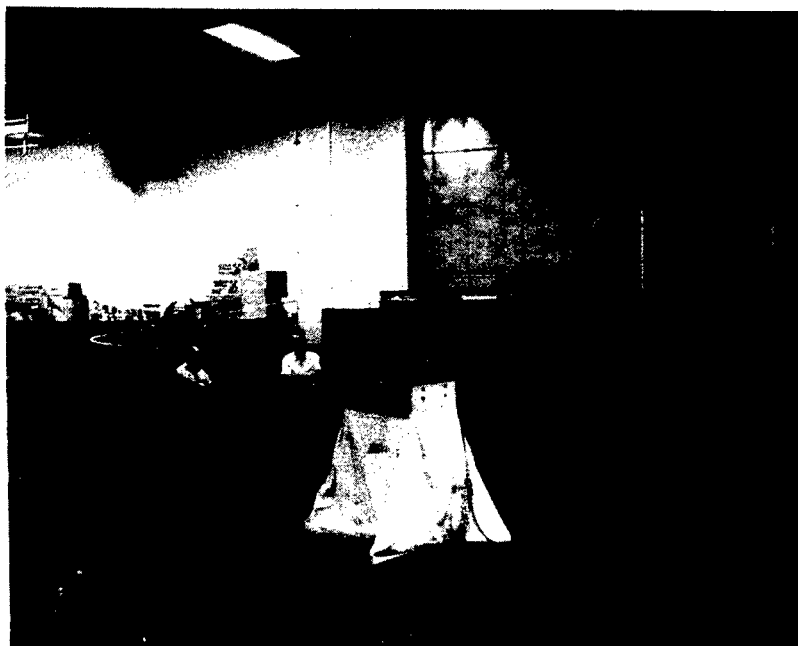Gondola

-Model Tower

Fig. 20   View of Overhead Camera

Fig. 21   View of Ground Camera Showing
Model in Operation

Run No.	Gondola Weight	Cable No.	Gondola Drag
4	W_1	C_2	D_1
5	W_2	C_2	D_1
6	W_3	C_2	D_1
7	W_1	C_1	D_2
8	W_2	C_1	D_2
9	W_3	C_1	D_2
10	W_1	C_2	D_2
11	W_2	C_2	D_2
12	W_3	C_2	D_2
13	W_1	C_1	D_3
14	W_2	C_1	D_3
15	W_3	C_1	D_3
16	W_1	C_2	D_3
17	W_2	C_2	D_3
18	W_3	C_2	D_3

The numerical values of the gondola weights, cable weights and dimensions of drag plates are listed in Table II. Each run consisted of measurements at 5 different speeds corresponding to cable angles $\varphi_o = 30°$, $40°$, $50°$, $60°$, $80°$. Each speed was run at least three times. Consequently the total sum of test points was over 270.

The procedure on each test point was as follows. The speed was so adjusted, that approximately the intended cable angle was obtained. For this purpose a protractor was used as shown in Fig. 19. The accurate speed was determined by means of a stop watch. The speed measurement was repeated before and after each measurement.

Next the air nozzle was adjusted so that a disturbance of suitable amplitude was obtained. The lights on the model were switched on and the lights of the test room switched off.

Turns were counted from one to seven. Shortly before "three" was pronounced, the airjet was turned on and the shutter of the cameras were opened. The air jet was closed as soon as the gondola had passed it. The shutters were left open up to "five" or "seven" respectively. The path of the undisturbed motion was recorded on a separate film. Examples of the pictures taken by the overhead and the ground camera are shown in Fig. 22 through 27.

Evaluation of the Tests

In order to evaluate the records taken by the overhead camera, enlarged prints of the size 14 x 14 inch were made and the deviations δ from the steady state path were measured and plotted versus the azimuth angle. In cases, where the shutter was left open until "seven" almost unsurmountable difficulties were met in following the trace through the many recorded turns. A plotting of 7 tests are shown in Fig. 27 and 28. These plots show the frequencies of the two pendulum modes and indicate that they are shorter than the turning period. The damping of the disturbances is so low that one might assume a slight instability, if eye observation had not indicated that the disturbances never increased, no matter how long the disturbances were observed.

The stability being so small one would expect to find some cases of instability if the weight of the gondola, the weight of the cable, the drag of the gondola, and the turning speed were varied. For all these variations, however, no change of stability was observed within the accuracy of the measurements. This result was considered a crucial and sufficient check of the theory.

The rotary motions described by the angles q_3 and q_4 could be observed in a small number of cases, (Fig. 26), which showed that these modes have a shorter period and high damping which causes their decay before the pendulum modes have reached their first maximum. This result justifies the separation of rotary and pendulum modes made in the theoretical investigations.

A detailed evaluation of the overhead camera pictures was considered not justifiable. Such an evaluation would have required a record which includes the undisturbed motion and a high number of turns after the disturbance. In order to discern between the different turns it would have been necessary to install a flicker mechanism in the circuit of the gondola bulb which produces different signals composed of dashes and dots. This installation was not made since the obtained qualitative checks of the theory were considered sufficient.
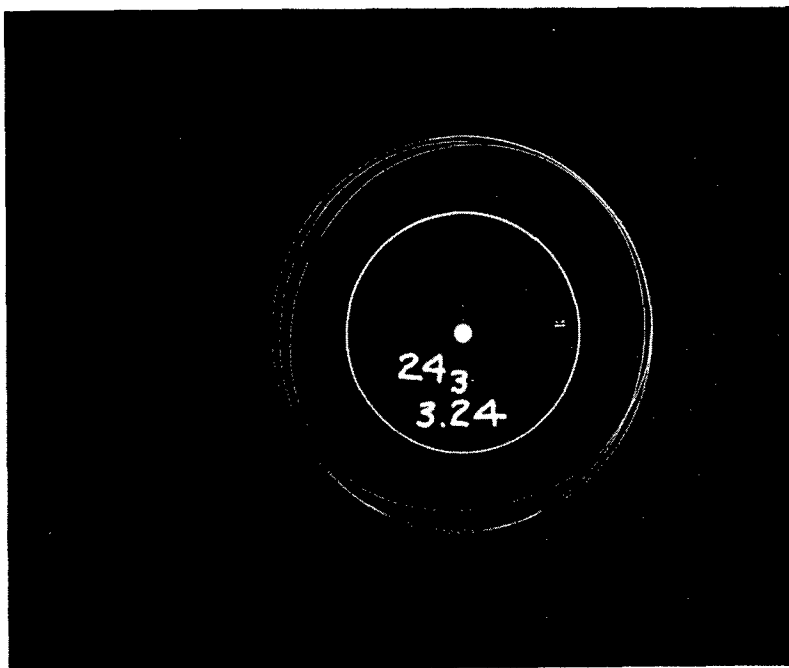
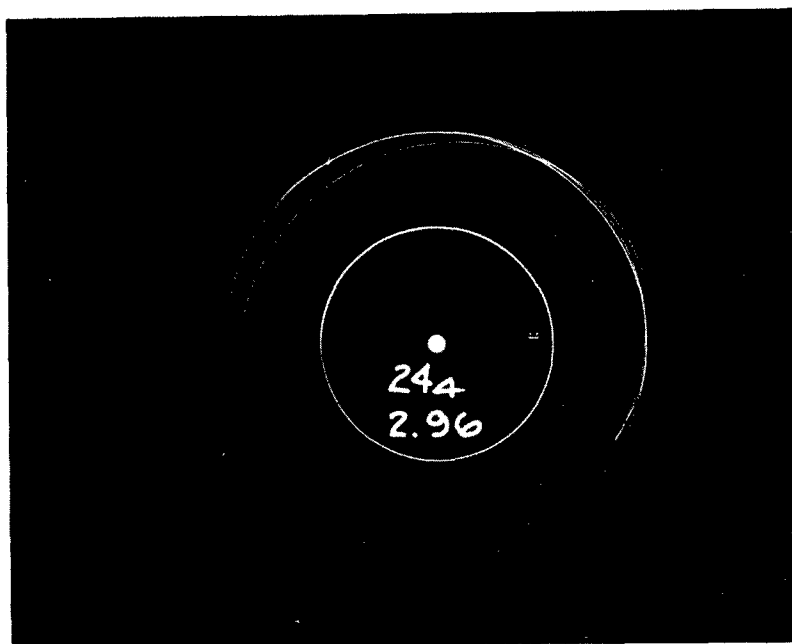Fig. 22 Record Taken by the Overhead Camera
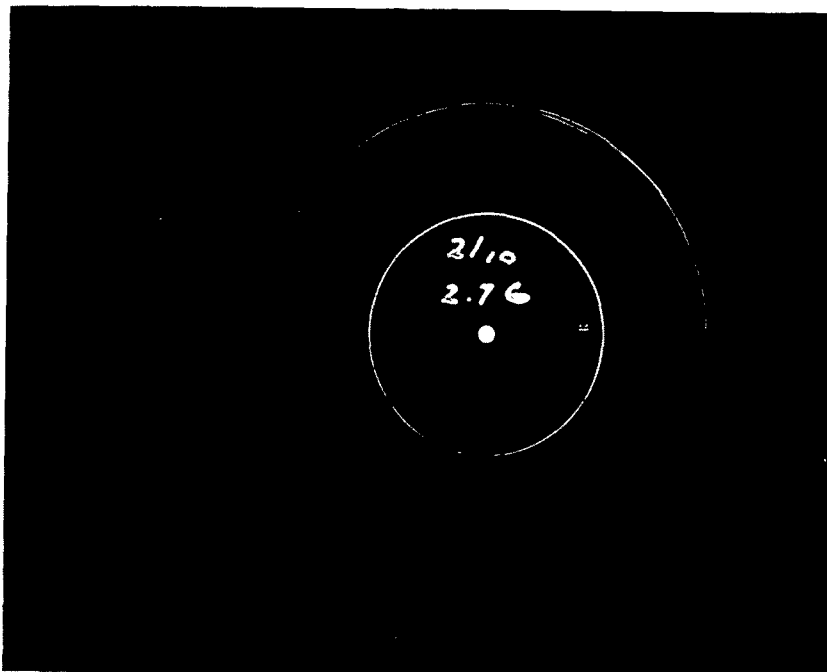

Fig. 23 Record Taken by the Overhead Camera

Fig. 24 Record Taken by the Overhead Camera
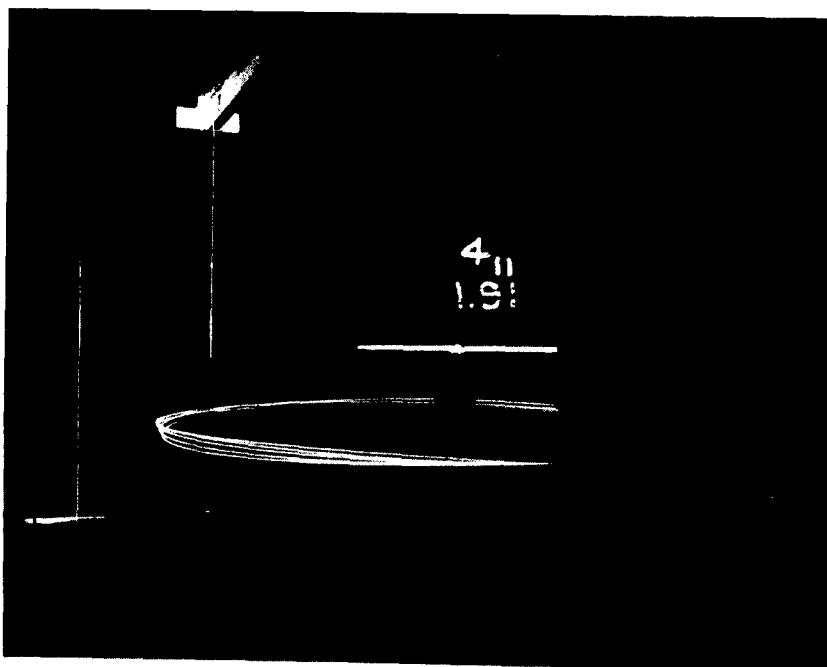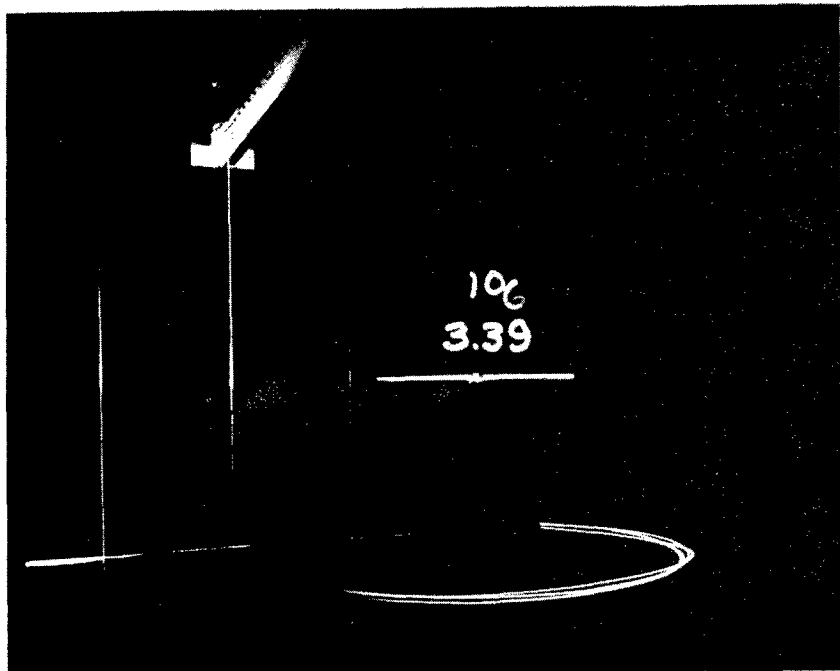

Fig. 25 Record Taken by the Floor Camera

Fig. 26   Record Taken by the Floor Camera

Explanation of the Observed Instability

Since the instability observed on the full scale equipment could neither be reproduced by the theory for a single point suspension nor by the corresponding model tests, the reason for the instability must be looked for in the difference between the single cable and the double cable suspension. This is the more obvious because the instability at 50 mph did not develop on the full scale equipment any more after the double cable suspension had been replaced by a single cable suspension. From an academic standpoint, an exact proof of this statement would be of interest.

A numerical investigation of this instability, however, meets the previously mentioned difficulties caused by the lack of the necessary data on initial twist and friction between the sheathing units. Since the Equipment Laboratory was not interested in such an investigation, it was not undertaken.

Conclusions and Recommendations

Based on the agreement between theory and tests, the following conclusions are drawn:

1. Regardless what the weight and drag of the gondola and of the cable might be, regardless of the length of the whirl arm and of the cable, and regardless of the whirling speed, the system is always stable if a one point suspension is used and if $C_D - \frac{\partial C_c}{\partial \beta} \geq 0$, i.e. if the drag is higher or equal to the slope of the cross force coefficient plotted versus angle of yaw.

2. A violation of this condition mentioned in point 1 seems to have a minor effect on the stability.

3. The observed instability was very likely caused by irregularities in the mounting of cable sheathing and by mutual interference between the aerodynamic forces on the two cable sheathings.

4. Because of the observed instability and because of the difficulties to be expected in a theoretical or experimental investigation of the double point suspension, a single point suspension is recommended.

5. From a stability standpoint an unsheathed cable of circular cross-section is the safest. Since, however, the high drag of such a cable would prevent the system reaching the required circumferential speed of 500 mph a sheathing should be applied, which is flutter safe and

has, under operational conditions, a torsional frequency high enough not to couple with the yawing motion of the gondola. This means the mass center of a unit length of cable and sheathing should be a few percent of the sheathing chord in front of the center of pressure and of the elastic axis.

6. The new gondola should have such a form that its slope of cross force coefficient versus angle of yaw is as small as possible. This means that the lateral projections of all surfaces, which produce cross forces, should be kept to a minimum. If there would be no drag restrictions a sphere would be the ideal form
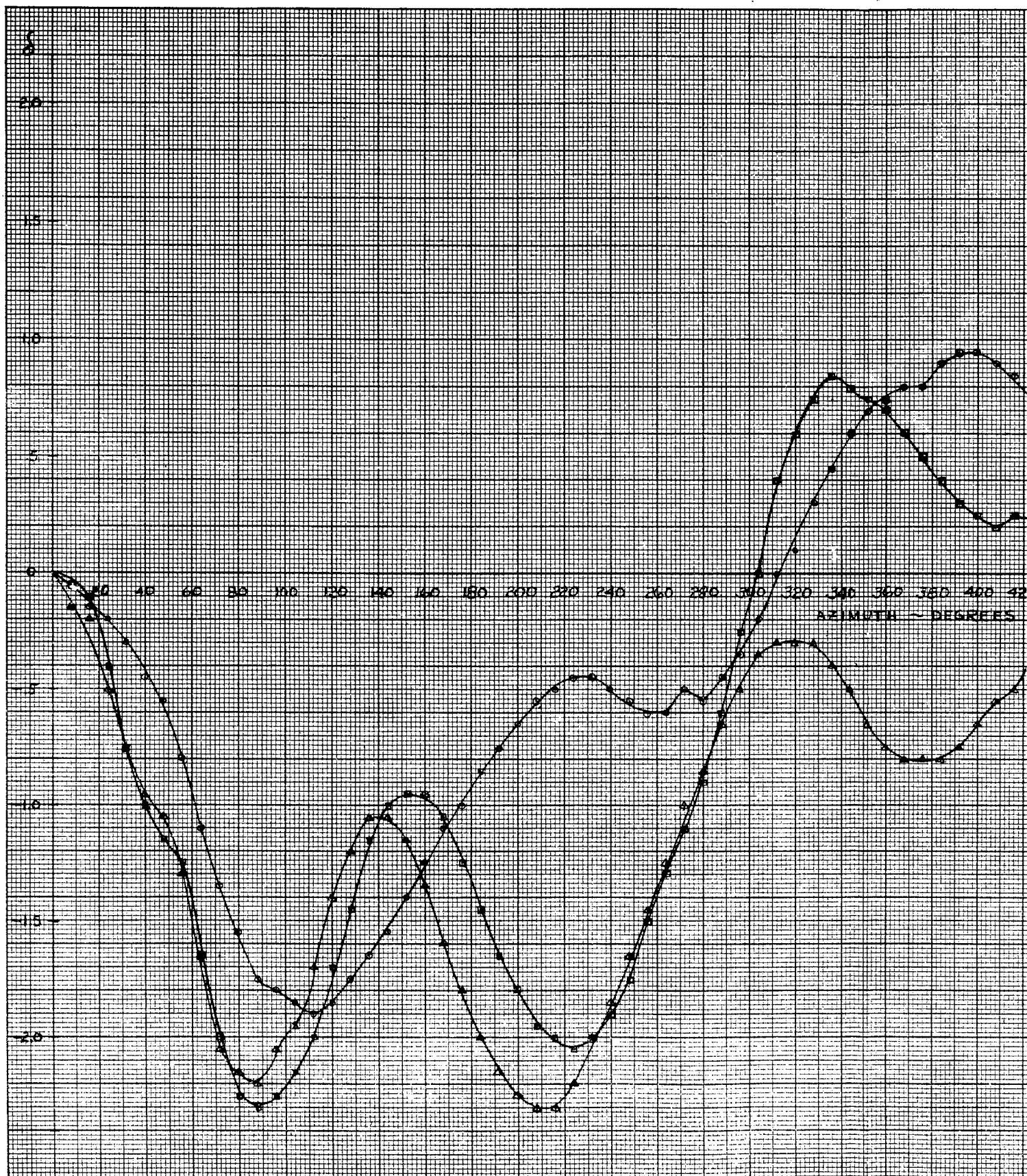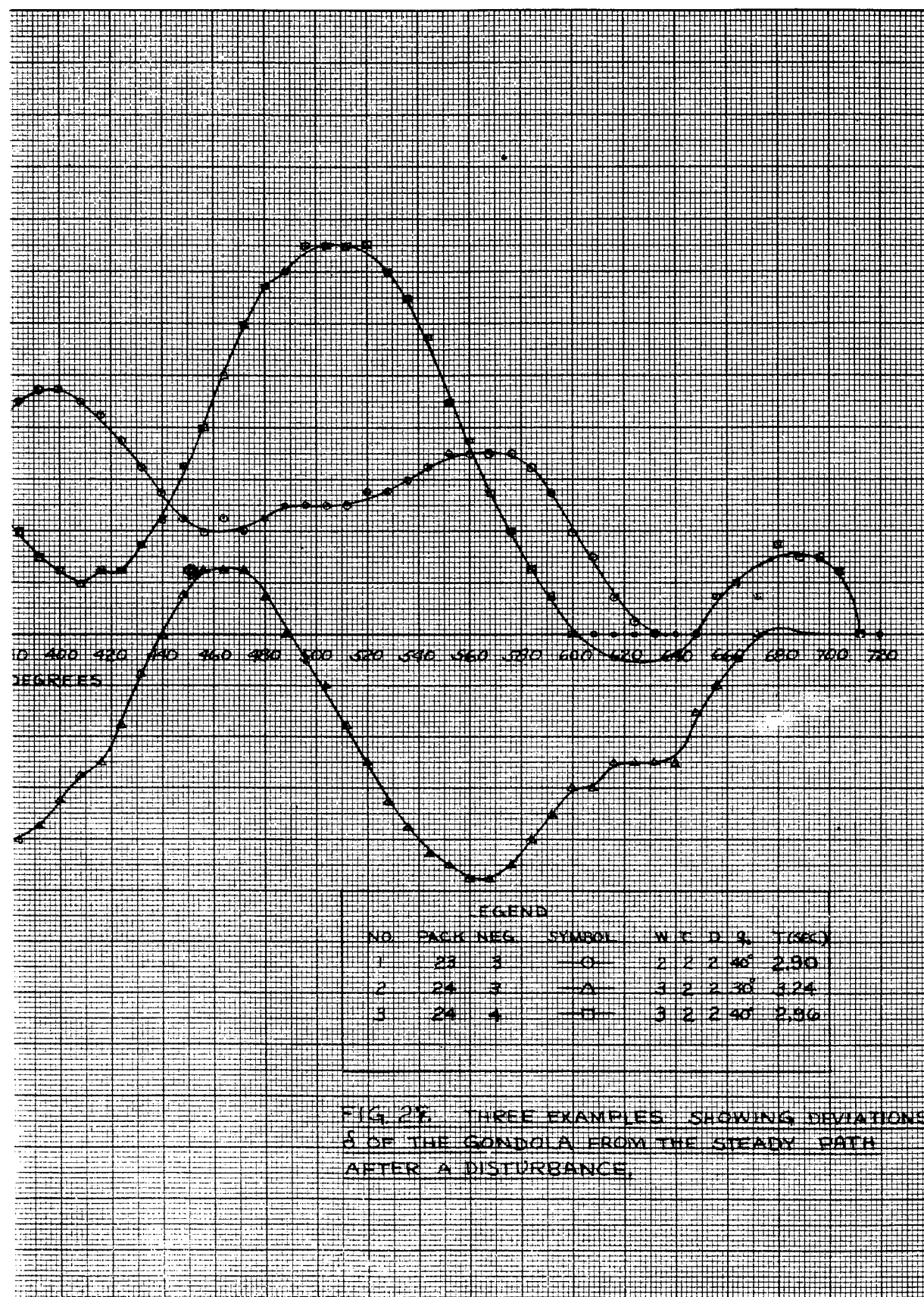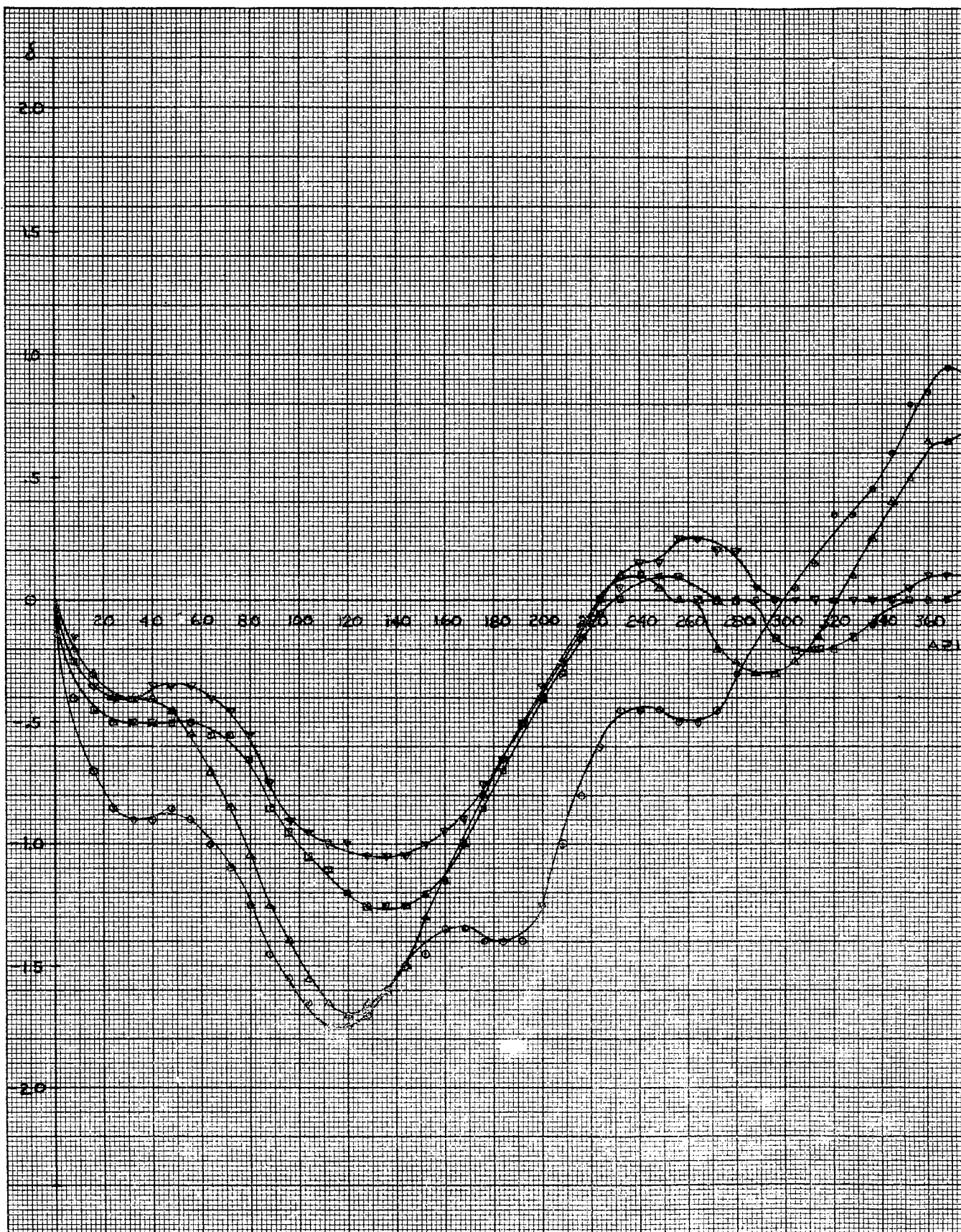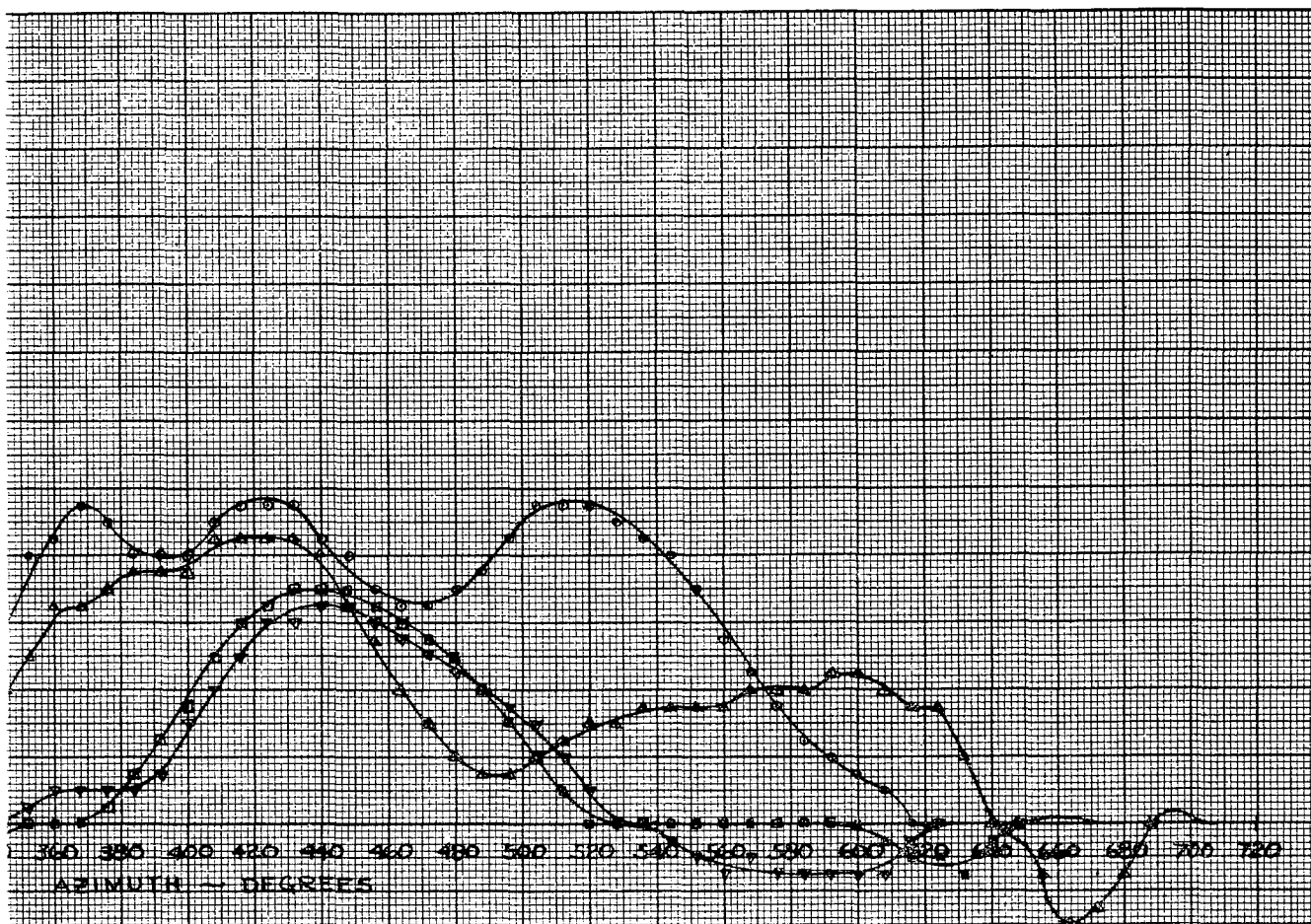
AZIMUTH — DEGREES

FIG. 2Y. THREE EXAMPLES SHOWING DEVIATIONS
δ OF THE GONDOLA FROM THE STEADY PATH
AFTER A DISTURBANCE.

			LEGEND						
NO.	PACK	NEG.	SYMBOL		W	C	D	θ	T (SEC)
1	23	5	—O—		2	2	2	40°	2.90
2	24	3	—A—		3	2	2	30°	3.24
3	24	4	—□—		3	2	2	40°	2.96

2

AZIMUTH — DEGREES

LEGEND

NO	PACK	NSR	SYMBOL	W	C	D	θ	Y
1	21	9	———○———	1	2	2	30°	3.20
2	21	10	———△———	1	2	2	40°	2.76
3	22		———◇———	1	2	2	50°	2.54
4	22		———▽———	1	2	2	60°	2.28

FIG. 20. FOUR EXAMPLES SHOWING DEVIATIONS Δ OF THE GONDOLA FROM THE STEADY PATH AFTER A DISTURBANCE.

②

TABLES

Table I

Data on the Full Scale Test Equipment
Used in Stability Calculations

Altitude of the tower . . . . 120 ft

Length of cables . . . . L = 116 ft

Length of Protruding Whirl Arm . . . . R = 56 ft

Weight of Gondola Including Parachute and Dummy . . . . mg = 685 lbs

Empty weight of Gondola Including Balancing Lead . . . . 405 lbs

Load of Gondola . . . . 280 lbs

Weight per ft of 6 Stranded Cables Without Sheathing. . . = 5.17 lb/ft

Weight per ft of 6 Stranded Cables With Sheathing. . . . g_{λ} = 6.27 lb/ft

Length of Gondola . . . . l = 8.5 ft

Cross Section Area of Gondola . . . . $\otimes$ = 3.14 ft^2

Center of Gravity of Gondola is Located at 41% of Length of Gondola

Slope of Pitching Moment Coefficient of Gondola . . . . $\frac{\partial C_m}{\partial \alpha}$ = 0.47

Nondimensional Pitching Moment Coefficient . . . . . . $\frac{\partial C_m}{\partial q_3'}$ = .001075

Drag Coefficient of Gondola Plus Cable . . . . C_D = 0.24

Gondola Mass Factor for Loaded Condition . . . . μ = 335

Mass Density of Air . . . . .002378 $\frac{\text{lb sec}^2}{\text{ft}^4}$

Maximum circumferential design speed . . . . V_{max} = 500 mph

Time Factor . . . . $\tau = \frac{2848.6}{V_o}$

Output of Driving Motor . . . . 2300 HP

Total Gearing Ratio From Motor Shaft to Whirl Arm. . . . 22:1

Table II

Numerical Data of the Model Test Equipment

Length Scale Factor . . . . Λ = 1:20

Time Scale . . . . 1: $\sqrt{20}$

Altitude of the Tower . . . . 6.0 ft

Length of Cables . . . . L = 5.8 ft

Length of Protruding Whirl Arm . . . . R = 2.8 ft

Gondola Weights . . . . W_1 = 17.9 gr
W_2 = 23.0 gr
W_3 = 38.8 gr

Weights of Cables . . . . W_{c_1} = 17.1 gr W_{c_2} = 34.2gr

Length of Gondola . . . . 5.6 inches

Cross Section Area of Gondola. . . . . 1.54 sq in.

Diameter of Drag Disks . . . . D_1 = 0
D_2 = 7/16"
D_3 = 7/8"

TABLE III

Coefficients and Solutions of the Frequency Polynominal Calculated With the Data of Table I

%	A_2	A_1	A_0	R	T sec	T_1 Uncoupled	Sec. Coupled	T_2 Uncoupled	Sec. Coupled	ξ_1	ξ_2
85	973	99	$.107 \times 10^6$	$.022 \times 10^4$	4.1	3.3	3.4	5.5	5.5	$.10 \times 10^{-6}$	$.56 \times 10^{-2}$
80	1042	103	$.117 \times 10^6$	$.093 \times 10^4$	5.8	4.7	4.6	7.6	7.2	$.30 \times 10^{-6}$	$.52 \times 10^{-2}$
75	1159	108	$.135 \times 10^6$	$.228 \times 10^4$	7.1	5.8	5.6	8.8	8.0	$.45 \times 10^{-6}$	$.46 \times 10^{-2}$
70	1331	117	$.162 \times 10^6$	$.458 \times 10^4$	8.3	6.8	6.3	9.5	8.3	$.48 \times 10^{-6}$	$.41 \times 10^{-2}$
65	1565	129	$.201 \times 10^6$	$.833 \times 10^4$	9.2	7.8	6.9	9.9	8.3	$.44 \times 10^{-6}$	$.36 \times 10^{-2}$
60	1875	144	$.256 \times 10^6$	1.43×10^4	10.1	8.7	7.4	10.0	8.2	$.36 \times 10^{-6}$	$.31 \times 10^{-2}$
55	2276	164	$.334 \times 10^6$	2.39×10^4	10.9	9.5	7.8	10.0	8.1	$.29 \times 10^{-6}$	$.27 \times 10^{-2}$
50	2797	190	$.447 \times 10^6$	3.91×10^4	11.8	10.4	8.1	9.9	7.9	$.21 \times 10^{-6}$	$.24 \times 10^{-2}$
45	3473	223	$.619 \times 10^6$	6.37×10^4	12.6	11.2	8.4	9.8	7.7	$.16 \times 10^{-6}$	$.21 \times 10^{-2}$
40	4364	267	$.893 \times 10^6$	10.37×10^4	13.4	12.0	8.7	9.7	7.6	$.12 \times 10^{-6}$	$.18 \times 10^{-2}$
35	5561	326	1.36×10^6	17.07×10^4	14.2	12.7	8.8	9.5	7.5	3.0×10^{-8}	$.16 \times 10^{-2}$
30	7225	408	2.24×10^6	28.7×10^4	15.1	13.2	9.0	9.3	7.4	5.5×10^{-8}	$.14 \times 10^{-2}$
25	9640	527	4.06×10^6	49.9×10^4	16.2	13.5	9.2	9.1	7.4	3.5×10^{-8}	$.12 \times 10^{-2}$
20	13370	709	8.40×10^6	91.1×10^4	17.5	13.5	9.5	8.9	7.4	2.2×10^{-8}	$.10 \times 10^{-2}$
15	19760	1020	21.1×10^6	181×10^4	19.4	13.3	9.8	8.7	7.5	1.2×10^{-8}	$.08 \times 10^{-2}$
10	32800	1640	71.7×10^6	415×10^4	22.7	12.8	10.0	8.5	7.5	$.54 \times 10^{-8}$	$.06 \times 10^{-2}$
5	72400	3510	468×10^6	1320×10^4	30.2	12.2	10.4	8.3	7.7	$.13 \times 10^{-8}$	$.04 \times 10^{-2}$